A STUDY OF $\pi\pi \to K\bar{K}$ USING AN EXPERIMENT ON $\pi^- p \to K^0_S K^0_S n$ AT 8.9 GeV/c *)

W. Wetzel[1], K. Freudenreich, F.X. Gentit[2] and P. Mühlemann[3]
ETH, Zurich, Switzerland

W. Beusch, A. Birman[4] and D. Websdale[5]
CERN, Geneva, Switzerland

P. Astbury, A. Harckham[6] and M. Letheren[7]
Imperial College, London, UK

ABSTRACT

We present an analysis of the $K^0_S K^0_S$ system, based on 6380 events, produced in the reactions $\pi^- p \to K^0_S K^0_S n$. Using a one-pion exchange model with absorption we determine the S- and D-wave amplitudes of $\pi\pi \to K\bar{K}$. Several A_2 production amplitudes were also included in the fits and we conclude that an unnatural parity exchange amplitude, which does not interfere with pion exchange, seems to be present. A branching ratio $\Gamma(f \to K\bar{K})/\Gamma(f \to \pi\pi) = 0.029 \pm 0.006$ is determined. With this and other new values of branching ratios we have fitted the $2^+ \to 0^-0^-$ decay rates to the SU(3) relations resulting in $(36.2 \pm 1)^\circ$ for the tensor nonet mixing angle.

Geneva - 19 May 1976

(Submitted to Nuclear Physics B)

---

*) Supported in part by the Swiss National Science Foundation.
Present addresses:
1) Institut für Theoretische Physik, Heidelberg, Germany;
2) CEN, Saclay, France;
3) University of Geneva, Geneva, Switzerland;
4) Dept. of Physics, Technion, Haifa, Israel;
5) Imperial College, London, UK;
6) Middlesbrough Polytechnic, Middlesbrough, UK;
7) CERN, Geneva, Switzerland.

1. INTRODUCTION

In this paper we present an analysis of the $K^0_S K^0_S$ system produced in the forward direction in the reaction $\pi^- p \to K^0_S K^0_S n$ at a beam momentum of 8.9 GeV/c. The purpose of the experiment was to investigate the production and decay of relatively high-mass resonances with low spin. Since the decay channel consists of indistinguishable particles, only the even partial waves are present. This simplification enables us to reach some conclusions with the relatively modest number of 6380 events.

The process $\pi^- p \to K^0 \bar{K}^0 n$ is complementary to $\pi^- p \to K^+ K^- n$ in so far as the isospin I = 1 $K\bar{K}$ resonances have amplitudes of opposite sign in the two cases. At our beam energy and at $K\bar{K}$ masses below 1.6 GeV the effective $n\bar{K}^0$ mass is above the region of prominent Y^* resonances. We may therefore picture the process as a scattering off the meson cloud of the target proton. The amplitude analysis we have performed shows, in fact, that π exchange is the dominant mechanism. The data therefore contain valuable information on the inelastic amplitude $\pi^+\pi^- \to K^0\bar{K}^0$. The paper is organized as follows. In Section 2 we discuss the experimental procedure, in particular the question of absolute cross-section normalization (including radiative corrections) and of corrections for the acceptance of the apparatus. The data, in the form of unnormalized moments and t-distributions, are presented in Section 3 where also their characteristic features are discussed. We interpret the data in terms of an absorptive one-pion exchange model, the details of which are presented in Section 4. The results of fitting this model to the data are given in Section 5. This pion exchange model gives a fair fit to the data over the full mass and t-region considered $[M \leq 1.6$ GeV, $|t| \leq 0.5$ GeV$^2]$. Near threshold our data represent a particularly pure sample of pion exchange, and in Section 6 we discuss our results in connection with those on the elastic $\pi\pi \to \pi\pi$ channel obtained from $\pi^- p \to \pi^+\pi^- n$. In the region of the f resonance we expect contributions of A_2^0 production to the $K^0_S K^0_S$ channel. We test the compatibility with our data of the various possible A_2^0 production amplitudes, of a magnitude derived from experiments on A_2^0 production. Models containing such amplitudes are in general compatible with our data and give better fits than the pure pion exchange model. A notable exception is, however, the m = 0 unnatural parity exchange amplitudes interfering with pion exchange. Towards the end of Section 6 we present our observations on the partial widths $\Gamma(f \to K\bar{K})$ and $\Gamma(f' \to \pi\pi)$, and we include them into a new fit of 2^+ nonet to 0^- nonet transitions.

2. EXPERIMENTAL PROCEDURE

The data on $\pi^- p \to K^0_S K^0_S n$ at 8.9 GeV/c were taken in an experiment performed at the CERN Proton Synchrotron (PS) using a large magnet spark chamber[1]. The set-up was very similar to the one already described[2]. The beam was defined by

a beam telescope containing two threshold Čerenkov counters for identifying the π^-. A veto counter (scintillator/Pb sandwich) surrounded the 41 cm long H_2 target almost completely. The trigger demanded an incident π^-, no signal in the veto counter, and at least one charged particle in a counter covering the downstream end of the spark chamber. Out of 116,000 photographs taken, about 12,750 showed a V^0V^0 topology. These were measured on a flying-spot digitizer HPD. The digitizings were processed through a chain of programs which performed track recognition, geometrical reconstruction and kinematic hypotheses testing. Most of the events that failed to satisfy one of the V^0 hypotheses ($K^0_S \to \pi^+\pi^-$, $\Lambda \to p\pi^-$, $\bar{\Lambda} \to \bar{p}\pi^+$, and $\gamma + Z \to e^+e^- + Z$) were measured manually. About 16% of the sample with V^0V^0 topology still failed to fit both V^0s (only about a quarter of these may be explained by K^0_L and $\pi^\pm$ decays). We accounted for this sample by a correction factor of 1.10 ± 0.1, where the upper error limit corresponds to the assumption that this unfit sample contains the same fraction of $K^0_SK^0_Sn$ final states as the sample of fits to both V^0.

The total correction factor for analysis loss, taking into account also unmeasurable photographs and other minor losses, was 1.175 ± 0.12. Smaller corrections were applied for accidental anticoincidences (1.03) and for scanning efficiency (1.02). A further correction, which is not usually applied in hadron physics, concerns radiative corrections. Loosely speaking, the charge of the incident fast π^- is annihilated in this reaction and this gives rise to the emission of bremsstrahlung. The photons are sharply peaked at an angle of about 15 mrad with respect to the beam direction and hit therefore a veto counter (Pb scintillator sandwich) at almost a right angle. The detection efficiency for such photons, η_γ, depends therefore only on their energy ω, a fact that simplifies the computation of radiative corrections for this experiment. We follow the treatment of Etim et al.[3] simplifying their general expression for the relation of measured cross-section σ_M to the "theoretical" cross-section σ by using $dP(\omega)$ (probability of photon emission in the interval $\omega \ldots \omega+d\omega$):

$$\sigma_M = \int dP(\omega) \left[1 - \eta_\gamma(\omega)\right] \times \sigma \ .$$

We use their approximation

$$dP(\omega) \simeq \beta \frac{d\omega}{\omega} \left(\frac{\omega}{E_\pi}\right)^\beta \ ,$$

where β is the result of an integration over all photon directions:

$$\beta = \frac{2}{\pi \cdot 137} \left(\ln \frac{2E_\pi}{\mu} - 1\right) = 0.01788 \ ,$$

E_π being the beam energy and μ the pion mass. The photon detection efficiency η_γ rises from threshold (0.37 MeV) to 8.5% at 1 MeV (Compton effect). At higher energy it is determined by pair creation and it reaches 84%. The result of the integration is

$$\sigma_{exp} = 0.896 \cdot \sigma \ .$$

We use a correction factor 1.114 ± 0.02, where the error reflects the uncertainty on $\eta_\gamma(\omega)$. The large size of this correction is partly due to the high detection efficiency of the veto counter. In the absence of a veto counter, the experiment would be sensitive to an energy imbalance greater than $\Delta E \simeq 300$ MeV, and in this case the correction would be about 6%. A corresponding correction has to be applied to experiments which observe $\pi^+\pi^-n$ and K^+K^-n final states with the same energy resolution (and a larger correction for a more performing apparatus).

By reconstruction of the K_S^0 trajectories it was possible to determine the interaction vertex with a precision of ±1 cm along the beam direction. Applying a cut on this coordinate we were able to remove all events produced downstream of the H_2 target. Comparing the effect of this cut to the distribution of events obtained with the hydrogen target empty, we determined a correction factor for this cut of 1.028. A further correction is needed for δ-rays produced by the incident π^- in the H_2 and triggering the veto counters (1.025 ± 0.01)

Other corrections depend on the configuration of the event and have been combined in a weight which is computed for each event. The solid angle of the apparatus is limited by the downstream trigger counter. Events are lost if none of the four pions of the K_S^0 decays hits this counter. This correction was studied by Monte Carlo simulation. It was found to be only about 8% on the average and not violently dependent on any variable describing the events; we parametrized it by a simple formula depending on the $K\bar{K}$ mass and on t. Events with both K_S^0 decaying downstream of the veto counter are therefore detected with more than 90% probability in the mass and t-range considered here. The largest contribution to the weight is produced by K_S^0 decays inside the veto counter. In order to reduce its fluctuations from event to event, we did not use the reconstructed interaction point for its evaluation, but we took an average over the target length weighted by the beam attenuation in the H_2. This correction factor is of the order of 10, but its relative systematic error is less than 3%. Other, smaller corrections, taken together in the weight, are made for: absorption of the incident π^- in the H_2, absorption of the K_S^0 in the H_2 and in the veto counter, and triggering of the veto counter by the recoil neutron. The extensive remeasurements by hand (2522 $K_S^0K_S^0n$ events) provide us with a check on possible biases introduced by the automatic measurement followed by pattern recognition. We did not find any bias except perhaps a loss of about 7% in the lowest 20 MeV of the $K_S^0K_S^0$ mass distribution.

We conclude that we do not expect any systematic error larger than 10% in any interval of t, $K^0_S K^0_S$ mass, or K^0_S angle within the domain of t and mass discussed here. One event with weight W represents a cross-section $W(1.06 \pm 0.11) \times 10^{-34}$ cm^2 for $\pi^- p \to K^0_S K^0_S n$ (all K^0_S decay modes). The channel cross-section for $|t| < 0.5$ GeV^2, $M(K^0_S K^0_S) < 1.6$ GeV is $\sigma = (6.1 \pm 0.7)$ μb.

The dependence of the weight on the $K^0_S K^0_S$ mass can be seen form Fig. 1 where we present the weighted and the unweighted mass distributions. In Fig. 2 we show the t′ dependence ($t' = t_{min} - t$) of the weight and also its dependence on cos θ (defined in the Gottfried-Jackson frame). The high weight at $|\cos\theta| \sim 1$ reflects the presence of a K^0_S that is slow in the laboratory and unlikely to survive the veto counter surrounding the target.

3. THE DATA

In Figs. 1 and 3 to 7 we show the unnormalized moments $\langle \mathrm{Re}\ Y^M_L \rangle$ of the $K^0_S K^0_S$ angular distribution in the Gottfried-Jackson frame. Choosing the y-axis normal to the production plane, the moments $\langle \mathrm{Im}\ Y^M_L \rangle$ should vanish by parity conservation; this is observed. The moments are plotted as a function of the $K^0_S K^0_S$ mass for two intervals of t: $|t| < 0.2$ and $0.2 \leq |t| < 0.5$ GeV^2. Since the acceptance is non-vanishing over the full angular range, we computed the moments simply by evaluating $\langle Y^M_L \rangle = \Sigma_i W_i\ Y^M_L(\theta_i, \phi_i)$, W_i being the weight of event i. The relation between moments and $K\bar{K}$ density matrix elements is given in the Appendix.

We observe that at small t the dominating moments are those with M = 0, as expected for π exchange. The absence of a significant signal in $\langle Y^0_6 \rangle$ and $\langle Y^0_8 \rangle$ indicates that only the ℓ = 0 and ℓ = 2 partial waves are important up to a mass $M(K^0_S K^0_S) = 1.6$ GeV. Since $\langle Y^0_4 \rangle$ vanishes near threshold, the observed enhancement in $\langle Y^0_0 \rangle$ is produced by the ℓ = 0 wave. Since no comparable enhancement exists in the reaction $\pi^- p \to K^- K^0 p$ [4], we conclude that it has ℓ = 0 and I = 0. With these quantum numbers it should represent a rather pure sample of π-exchange events.

The other prominent feature in our data is a resonance structure around $M(K^0_S K^0_S) = 1.3$ GeV. The occurrence in the moment $\langle Y^0_4 \rangle$ and its mass identify it as f and/or A_2. Since only the f can be produced by pion exchange, f is favoured if the data indicate dominant pion exchange also in this region. We note a qualitative evidence for this by considering the t-distribution and the energy dependence. In Fig. 8 we show $(\mu^2 - t)^2\ d\sigma/dt'$, μ being the pion mass and $t' = t - t_{min}$, for the two mass intervals $M(K\bar{K}) < 1.05$ GeV and $1.3 \leq M(K\bar{K}) \leq 1.35$ GeV. Both distributions are quite similar and show an approximately linear rise for small t as expected for pion exchange. In Fig. 9 we show the dependence on beam momentum of the cross-section for $\pi^- p \to K^0_S K^0_S n$ in the region $0 < |t| < 0.5$ GeV^2 and for the mass bins indicated in the figure. We have obtained these cross-sections in this and

previous experiments[5,6]. Within the large errors, the energy dependence of pion exchange p_{lab}^{-2} is compatible with the data for masses $M(K\bar{K}) < 1.3$ GeV. A less steep energy dependence at higher masses does not necessarily indicate the absence of pion exchange; we have possibly underestimated the acceptance corrections of high-mass events in the previous experiments at lower beam momentum. The main features of the data considered so far are compatible with the dominance of π exchange in this reaction. Owing to absorption, pion exchange is expected to generate M = 1 moments which have essentially the mass dependence of the M = 0 moments but the opposite sign. This is indeed observed (see Figs. 3 and 4) for $\langle Y_2^1 \rangle$ and $\langle Y_4^1 \rangle$ with the exception of the $1.34 < M(K\bar{K}) < 1.44$ GeV region where $\langle Y_4^1 \rangle$ appears to become positive.

Peaks or shoulders in the mass distribution have also been observed in this region in previous experiments[5,6]. From the present analysis we conclude that the shoulder in the mass distribution (see Fig. 1a) is related to a rapid drop of the s-wave. The anomaly in $\langle Y_4^1 \rangle$ will be discussed in Section 6.5 in relation to A_2 production.

4. THE MODEL

The qualitative analysis presented in the preceding section justifies the use of a pion exchange model with absorption. Moreover, such models have been used successfully to describe the amplitudes in $\pi^- p \to \pi^+\pi^- p$ [7] at small t ($|t| \lesssim 0.15$ GeV^2). In this process, exchanges other than pion exchange become significant only at larger momentum transfer. The parametrization of a possible A_2 production will be discussed below.

In our notation ℓ and m describe the $K_S^0 K_S^0$ angular momentum in the Gottfried-Jackson frame, while λ_i and λ_f are the initial and final nucleon helicities; $\overset{\pm}{F}$ are amplitudes of defined exchange parity.

$$\overset{\pm}{F}{}^{\ell,m}_{\lambda_f,\lambda_i} = \frac{1}{2}\left[F^{\ell,m}_{\lambda_f,\lambda_i} \mp (-1)^m F^{\ell,-m}_{\lambda_f,\lambda_i}\right].$$

The amplitudes F contain a pion pole term and a cut term whenever they may contribute. The cut terms describing absorptive corrections are derived with the assumption that the absorption affects the two s-channel amplitudes $H_{+-}^{2,1}$ and $H_{+-}^{2,2}$ [8]. Denoting these contributions by $-F_D C_1$ and $-F_D C_2$ respectively, we have the following cut amplitudes in the Gottfried-Jackson frame (with the crossing angle χ defined in the Appendix):

$$\bar{F}^{2,0}_{+-}\ (\text{cut}) = -F_D\left[\frac{1}{2} C_1 \sqrt{6} \sin\chi \cos\chi + \frac{1}{2} C_2 \sqrt{\frac{3}{2}} \sin^2\chi\right]$$

$$\overset{+}{F}{}^{2,1}_{+-}\ (\text{cut}) = -F_D\left[\frac{1}{2} C_1 \cos\chi + \frac{1}{2} C_2 \sin\chi\right]$$

$$\bar{F}^{2,1}_{+-}\ (\text{cut}) = -F_D\left[\frac{1}{2} C_1 (2\cos^2\chi - 1) + \frac{1}{2} C_2 \sin\chi \cos\chi\right]$$

$$\overset{+}{F}{}^{2,2}_{+-}\ (\text{cut}) = -F_D\left[\frac{1}{2} C_1 (-\sin\chi) + \frac{1}{2} C_2 \cos\chi\right]$$

$$\bar{F}^{2,2}_{+-}\ (\text{cut}) = -F_D\left[\frac{1}{2} C_1 (-\sin\chi\cos\chi) + \frac{1}{4} C_2 (\cos^2\chi + 1)\right] .$$

We have observed that the contributions to the cut from $H^{2,1}_{+-}$ alone (i.e. $C_2=0$) do not lead to a satisfactory description of the $M \neq 0$ moments in the large t-region. This can be traced back to a change of sign of $2\cos^2\chi - 1$ at $t \simeq -0.3\ M^2(K^0_S K^0_S)$ and to the m = 2 terms being too large. Both features can be corrected for by the inclusion of the C_2 term. We have used, however, the empirical relation $C_1 = C\cos\chi$ and $C_2 = C\sin\chi$ which we found compatible with the results of the analysis of $\pi^- p \to \pi^+\pi^- n$ [9]. In this way a smooth cut contribution to $\overset{+}{F}{}^{2,1}$ and small amplitudes $\overset{\pm}{F}{}^{2,2}$ can be obtained without introducing more parameters. Measuring C in units of the Williams cut[10],

$$\left.\frac{d^2_{01}}{\sqrt{-t'}}\right|_{t=\mu^2} = \sqrt{\frac{3}{2}} \left.\frac{\sin\chi\cos\chi}{\sqrt{-t'}}\right|_{t=\mu^2}$$

and providing it with an exponential t-dependence then leads to the cut terms (with the strength parameter C as a factor) in the amplitudes given in Eqs. (1). The pion exchange terms are of standard form involving $1/(\mu^2 - t)$ and have in addition an exponential t-dependence. The expressions for nucleon flip amplitudes are:

$$\bar{F}^{0,0}_{+-} = F_S \frac{\sqrt{-t'}}{\mu^2 - t} e^{-b_S(\mu^2 - t)}$$

$$\bar{F}^{2,0}_{+-} = F_D\left[\frac{\sqrt{-t'}}{\mu^2 - t} e^{-b_D(\mu^2 - t)} - C \left.\frac{d^2_{01}}{\sqrt{-t'}}\right|_{t=\mu^2} \sqrt{\frac{3}{2}} \sin\chi \left(1 - \frac{\sin^2\chi}{2}\right) e^{-b_C(\mu^2 - t)}\right]$$

$$\overset{+}{F}{}^{2,1}_{+-} = F_D\left(-\frac{C}{2}\right) \left.\frac{d^2_{01}}{\sqrt{-t'}}\right|_{t=\mu^2} e^{-b_C(\mu^2 - t)} \qquad (1)$$

$$\bar{F}^{2,1}_{+-} = F_D\left(-\frac{C}{2}\right) \left.\frac{d^2_{01}}{\sqrt{-t'}}\right|_{t=\mu^2} \cos^3\chi\ e^{-b_C(\mu^2 - t)}$$

$$\overset{+}{F}{}^{2,2}_{+-} = 0$$

$$\bar{F}^{2,2}_{+-} = F_D\left(-\frac{C}{2}\right) \left.\frac{d^2_{01}}{\sqrt{-t'}}\right|_{t=\mu^2} \frac{1}{2} \sin^3\chi\ e^{-b_C(\mu^2 - t)} .$$

The amplitudes of Eqs. (2) give the (small) terms of nucleon non-flip:

$$\bar{F}^{0,0}_{++} = F_S \frac{\sqrt{-t_{min}}}{\mu^2-t} e^{-b_S(\mu^2-t)}$$
$$\bar{F}^{2,0}_{++} = F_D \frac{\sqrt{-t_{min}}}{\mu^2-t} e^{-b_D(\mu^2-t)} \quad . \tag{2}$$

This model has the following essential features:

i) $\bar{F}^{2,1}$ is in phase with $\bar{F}^{2,0}$; ii) $|\bar{F}^{2,1}_{+}| \geq |\bar{F}^{2,1}_{-}|$; iii) m = 2 states are negligible except for a small $\bar{F}^{2,2}$ term; and iv) $\bar{F}^{2,0}$ has, in addition to the pole term, a cut term related to the m = 1 amplitudes. Property (ii) is consistent with magnitude and sign of $\langle Y^2_2 \rangle$ and $\langle Y^2_4 \rangle$; (iii) explains the small inequality of $\langle Y^2_2 \rangle$ and $\langle Y^2_4 \rangle$ at larger t-values; (iv) is typical for an absorption model.

5. RESULTS OF FITTING THE MODEL

5.1 Mass independent analysis

The mass region from threshold to 1.65 GeV was divided into bins of 50 MeV (54 MeV for the first bin). F_S and F_D were parametrized in terms of the I = 0, $\pi\pi \to K\bar{K}$ S- and D-wave amplitudes, S and D, whose unitarity condition is $|S|^2 \leq 1$ and $|D|^2 \leq 1$. The relation between F_S, F_D, and S, D is given in the Appendix together with the expression of the differential cross-section in terms of the amplitudes $F^{\ell,m}_{\lambda_f,\lambda_i}$. The free parameters of the maximum likelihood fit were: the magnitudes $|S|$ and $|D|$, the phase difference $\phi_S - \phi_D$, the cut parameter C and the slope parameters b_S and b_D. The best fit results for $|t| \leq 0.5$ GeV^2 are shown in Fig. 10. The mass bin from 1.35 to 1.40 GeV needed a particular treatment since, $\langle Y^1_4 \rangle$ being positive as already noted above, the amplitudes of Eqs. (1) and (2) result in an unacceptable fit. Since $\langle Y^1_4 \rangle$ is mainly the interference term $\bar{F}^{2,0}_{+-} \cdot \bar{F}^{2,1*}_{+-}$, and since there is no evidence for an anomaly in $\bar{F}^{2,0}_{+-}$ (see $\langle Y^0_4 \rangle$, $\langle Y^0_2 \rangle$) we assume the anomaly to be produced by $\bar{F}^{2,1}_{+-}$. For this mass bin, we keep C a free parameter in $\bar{F}^{2,1}_{+-}$ only and fix C, for all other amplitudes, at 0.375, its value found in the neighbouring bins. The best fit parameters shown in Fig. 10 were obtained in this condition.

The slope parameter b_C of the cut term was fixed to $b_C = 0$ as determined in the mass-dependent fit described below. The phase difference, $\phi_S - \phi_D$, derived from $\cos(\phi_S - \phi_D)$ has, of course, two solutions symmetric about 180°; we show only the lower branch. We have also tested the presence of a $\ell = 4$ wave produced via pion exchange. For this purpose we have added to the model [Eqs. (1) and (2)] the amplitudes

$$\bar{F}^{4,0}_{+-} = F_G \frac{\sqrt{-t'}}{\mu^2 - t} \quad \text{and} \quad \bar{F}^{4,0}_{++} = F_G \frac{\sqrt{-t_{min}}}{\mu^2 - t} .$$

A fit to the data shows that the $\ell = 4$ wave is indeed negligible in the mass region discussed here.

5.2 Mass-dependent analysis

We also examined certain mass-dependent parametrizations in the threshold and resonance region based on the results obtained in Section 5.1.

5.2.1 Resonance region

We have used a mass-dependent parametrization to describe a resonant D-wave and an S-wave which falls above $M(K^0_S K^0_S) = 1.45$ GeV. Specifically, we used

$$D = \frac{2m_f \sqrt{\Gamma^{\pi}_f(M) \cdot \Gamma^{K}_f(M)}}{m_f^2 - M^2 - i m_f \Gamma_f(M)} \tag{3}$$

$$|S|^2 = S_0^2 \left[\frac{1 - \varepsilon}{1 + \exp\{4(M - m_S)/\Gamma_S\}} + \varepsilon \right] \tag{4}$$

$$\phi_S = \arg(S) = \phi_1 + \phi_2 \, (M - 2m_{K^0})/2m_{K^0} . \tag{5}$$

The expressions (4) and (5) which specify the S-wave are a purely empirical ansatz. The dependence of the partial widths Γ^{π}_f and Γ^{K}_f on the $K^0_S K^0_S$ mass M is given in the Appendix. The parameters C, b_S, b_D and b_C were constants in the fit. The result of this fit, done for $1.17 \leq M \leq 1.60$ GeV, is also given in Table 1; it is displayed as a continuous line in Figs. 1, 3 to 7, and 10. In Fig. 11 the t-dependence of the model is compared with the data in three suitable linear combinations of the moments $\langle Y^0_0 \rangle$, $\langle Y^0_2 \rangle$, and $\langle Y^0_4 \rangle$ (see Appendix for their definition).

5.2.2 Threshold region

In this region the S-wave is parametrized by a complex scattering length a and by the phase ϕ^0_S at threshold:

$$|S|^2 = \frac{4 q_K \, \mathrm{Im}\, a}{1 + 2 q_K \, \mathrm{Im}\, a + q_K^2 |a|^2} \tag{6}$$

$$\phi_S = \phi^0_S + \arctan\left(\frac{q_K \, \mathrm{Re}\, a}{1 + q_K \, \mathrm{Im}\, a}\right) , \tag{7}$$

where q_K is the K^0_S momentum in the $K\bar{K}$ rest frame. The D-wave is assumed to be the low mass tail of the f resonance [see its parametrization Eq. (3)] and b_D, b_C were fixed to the values found in 5.2.1. The parameters C, b_S are again

constants. Table 2 contains the best fit values obtained in the maximum likelihood fit in the region $M \leq 1.17$ GeV and $|t| \leq 0.5$ GeV^2. Re (a) was restricted to be negative. The result of this fit is also shown in Figs. 1, 3 to 7, and 10 (dotted line). The t-dependence of this parametrization fitted to the data is shown in Fig. 12. A reasonable agreement is observed throughout the threshold region. As expected from the smallness of the D-wave in the threshold region (see also mass-independent analysis), the phase $\phi_S - \phi_D$ is very badly determined there. We cannot, therefore, test it against the phase variation of the scattering length Eq. (7); in fact, a constant phase would be an equally good fit.

6. DISCUSSION OF THE RESULTS

Our results can be related to $\pi^- p \to \pi^+\pi^- n$, in which channel a very high statistics experiment has been reported[11] and, more directly, to $\pi^- p \to K^+K^- n$ [12,13]. In contrast to these channels our experiment contains only even partial waves and should therefore yield less ambiguous results. Moreover, the acceptance of our apparatus is more uniform than that of the spectrometer set-up used in $\pi^+\pi^-$ and K^+K^- experiments.

6.1 Inelasticity of the $\pi\pi$ scattering in the $K\bar{K}$ threshold region

Studies of the reaction $\pi^- p \to \pi^+\pi^- n$ [7,11] and $\pi^+ p \to \pi^+\pi^-\Delta^{++}$ [14] have shown that the $\pi\pi$ S-wave varies rapidly in the vicinity of the $K\bar{K}$ threshold, above which the elasticity η drops to less than 0.5. One expects therefore $|S|^2$ to reach values of the order of 0.75 since a) only the $K\bar{K}$ channel seems to be involved, and b) the $K\bar{K}$ S-wave at threshold is mainly I = 0 (see also Section 3). We find, however, a peak value of only $|S|^2 = 0.39 \pm 0.05$ in both the mass-dependent and mass-independent fits.

According to more recent analyses[15,16] of the data of Ref. 11, η does not show the strong decrease found in earlier studies[7,11]. In fact, the new values compare well with our estimate of $|S|^2$.

The estimates of $\sigma(\pi^+\pi^- \to K^+K^-)$ [12,14], expressed in terms of $|S|^2$, are in general higher than $|S|^2$ derived in this experiment. There is also a notable difference between $\langle Y_2^0 \rangle$ in $K_S^0K_S^0$ and $\langle Y_2^0 \rangle$ in K^+K^-. From Fig. 3 we note that $\langle Y_2^0 \rangle$ has a strong negative signal at 1.15 GeV of almost half the magnitude of $\langle Y_0^0 \rangle$. Such a signal is not observed in the moment $\langle Y_2^0 \rangle$ of the K^+K^- state[12,13]. Since the P-wave gives a positive contribution to $\langle Y_2^0 \rangle$, a sizeable P-wave may explain the difference in the moment $\langle Y_2^0 \rangle$; it also tends to increase $\sigma(\pi^+\pi^- \to K^+K^-)$ with respect to $\sigma(\pi^+\pi^- \to K_S^0K_S^0)$. It is however, improbable that the P-wave is responsible for the difference of the two cross-sections just above threshold. The shape of our mass spectrum in the threshold region, however, is similar to the K^+K^-

spectrum of Refs. 12 and 13. All $K\bar{K}$ mass spectra have peaks that are less sharp and that are higher above threshold than expected from a K-matrix analysis of the $\pi\pi$ data[7,11,12]. Since the position of the maximum moves up in mass with decreasing scattering length $|a|$, the $K\bar{K}$ data must result in a smaller value of $|a|$ than the $\pi\pi$ data.

6.2 The phase of the isoscalar S-wave

As long as the $K\bar{K}$ channel can be considered to be the predominant inelastic channel of the $\pi\pi$ S-wave in I = 0, the following relation (modulo π) holds between the phase of this channel ϕ_S and the $\pi\pi$ and $K\bar{K}$ scattering phase shifts $\delta_0^0(\pi\pi)$ and $\delta_0^0(KK)$, respectively:

$$\phi_S = \delta_0^0(\pi\pi) + \delta_0^0(KK) + m\cdot\pi \ . \tag{8}$$

In order to determine m we consider the $K\bar{K}$ threshold where Eq. (8) reduces to

$$\phi_S(th) = \delta_0^0(\pi\pi) + m\cdot\pi \ . \tag{9}$$

For an estimate of $\phi_S(th)$ we either extrapolate the mass independent fit values of $\phi_S-\phi_D$ to threshold or we use the scattering length ansatz for this purpose. The result of both methods lies within $150^\circ \leq \phi_S(th) \leq 250^\circ$, where the lower limit corresponds to Re a > 0. We have assumed here that ϕ_D is given by the resonance tail of the f meson according to Eq. (3). An additional minus sign in Eq. (3) [uncertainty of this sign would lead to another modulo π ambiguity in Eq. (8)] is excluded by the SU(3) analysis[17] of the $2^+ \to 0^-0^-$ decay rates from which it follows that the amplitudes for $f \to \pi\pi$ and for $f \to K\bar{K}$ have the same sign. By comparison with the $\pi\pi$ phase shift results[7,11,14-16] $\delta_0^0(\pi\pi, 1\ \text{GeV}) \hat{=} 180^\circ$, we conclude that we have to choose m = 0. If the S-wave near threshold is assumed to be related to the S^*, a member of the 0^+ nonet, this result implies that also the $S^* \to K\bar{K}$ amplitudes has the same sign as the $S^* \to \pi\pi$ amplitude. We now use Eq. (8) with m = 0 to determine ϕ_S at a mass where it is least affected by the ambiguity of $\phi_S-\phi_D$. Figure 10 shows that $|S|^2$ is constant from 1.1 to 1.25 GeV. It was established by fits similar to those described in Sections 5.2.1 and 5.2.2 that indeed no mass dependence is required for the S-wave. The phase value found in this region is $\phi_S = 190^\circ \pm 10^\circ$. At M = 1.1 GeV, ϕ_D is about 15°. Taking into account, for the error limits, the ambiguity of $\phi_S-\phi_D$ we therefore conclude that

$$180^\circ \leq \phi_S \leq 210^\circ \quad \text{at M = 1.1 GeV} \ .$$

With the use of Eq. (8) we can, given $\delta_0^0(\pi\pi)$, determine $\delta_0^0(KK)$. The recent $\pi\pi$ phase-shift analysis presents two different solutions at 1.1 GeV with $\delta_0^0(\pi\pi) \simeq 245^\circ$ and $\simeq 200^\circ$. With these two values we find, respectively,

$$-65^\circ \leq \delta_0^0(KK) \leq -35^\circ$$

and

$$-20^\circ \leq \delta_0^0(KK) \leq +10^\circ \ .$$

Conversely, from the scattering length fit [see Eq. (6)] wnich determines Im a and |a| we can evaluate $\delta_0^0(KK)$ and predict $\delta_0^0(\pi\pi)$. We find $\delta_0^0(KK) = -55°$ or $= +55°$ for Re a < 0 or Re a > 0, respectively. The increment of $\delta_0^0(\pi\pi)$ above threshold has its sign opposite to that of $\delta_0^0(KK)$. Since the $\pi\pi$ phase shift increases in this region, we prefer Re a < 0 and conclude from Eq. (8) that

$$235° \leq \delta_0^0(\pi\pi) \leq 265° \quad \text{at } M = 1.1 \text{ GeV} .$$

6.3 The S-wave above 1.1 GeV

The magnitude of the S-wave (Fig. 10) does not fall off above the threshold region but has a comparable value up to M = 1.4 GeV. This behaviour disagrees with those $\pi\pi$ phase-shift results for which the elasticity increases rapidly from the dip above the threshold to the f region[7,11]. From the smallness of the background under the A_2 peak in $\pi^- p \to K^- K^0 p$ [4] which is pure I = 1, we conclude that this difference can probably not be explained by an I = 1 contribution to $K_S^0 K_S^0$. In fact, some of the recent phase-shift solutions already mentioned[15,16] show a mass dependence of the elasticity up to 1.4 GeV which is quite compatible with the behaviour of the S-wave we observe.

6.4 S-wave slope and absorptive corrections

Our S-wave slope b_S is well determined in the threshold region, which is almost purely S-wave (see Fig. 10). The slope is considerably below the value of about 4.5 $(GeV/c)^{-2}$ found in a phase coherent analysis of the $\pi\pi \to \pi\pi$ channel[7] at 17.2 GeV/c. The difference is too large to be explained by shrinkage of the π exchange. We agree, however, with the value of the cut strength C found in elastic $\pi\pi$ scattering[7]. As seen in Fig. 10, the fit requires a value for C which decreases from threshold to the f region.

6.5 D-wave production

From the qualitative analysis presented in Section 3 and from the goodness of the fit 5.2.1 we conclude that a possible A_2 contribution to the D-wave has to be considerably smaller than that of the f. Since there are a number of possible amplitudes for A_2 production, interfering with f production amplitudes, we cannot determine them within the statistics of our data. In this situation we use experiments where $A_2^0 \to \rho\pi$ has been observed, in order to estimate the amount of A_2 production in our experiment. We then check whether the corresponding A_2 signal is compatible with our data. By doing this we also hope to improve our fit in two respects: a better description of the anomaly in $\langle Y_4^1 \rangle$ (discussed in Section 3) and better agreement of our f resonance parameters with those obtained in $\pi^- p \to$ $\to \pi^+ \pi^- n$ (where the A_2 is absent). We find our resonance mass about 10 MeV higher and the width about 25 MeV lower than those estimated for the f by Estabrooks et al. [7]. These differences might be significant because we used

the same method of analysis, in particular the same formula for the energy dependence of the partial widths (see Appendix) of Ref. 7*).

To our knowledge the most detailed results on A_2^0 production have been obtained in the charge symmetric process $\pi^+n \to A_2^0p$ at 4 GeV/c [18]. We scale from 4 GeV/c to our beam momentum using p_{lab}^{-2} for unnatural parity exchange and p_{lab}^{-1} for natural parity exchange. An energy dependence of p_{lab}^{-2} has been found for the cross-section of A_2 production with charge exchange [19]; the same energy dependence was found for the fraction of the charged A_2 production cross-section induced by unnatural parity exchange [20]. The observation that I = 0 exchange is mostly of natural parity while I = 1 exchange tends to be of unnatural parity [21] together with $\sigma(\text{unnatural}) \propto p_{lab}^{-2}$ [20] confirms the result of Ref. 19.

To get an impression of the size of the A_2 production, we have computed the t distribution of the moment combination M_1 under the assumption that the D-wave is due only to A_2 production in the mass interval $1.27 < M(K\bar{K}) < 1.37$ GeV. The result is shown in Fig. 11 as a dotted line. We have obtained this result by replacing the density matrix element ρ_{00}^{22} of fit 5.2.1 with the corresponding quantity for A_2 production derived**) from the 4 GeV/c π^+n experiment [18]. This unnatural parity A_2 production is seen to be non-negligible; its relative size increases with $|t|$.

We shall now discuss the compatibility of the following four possible A_2 production amplitudes with our data:

i) A_2 production, m = 0, by B exchange interfering with the dominant π exchange;

ii) f production via A_2 exchange and A_2 production via ρ exchange, m = 1, interfering with each other and with the pion cut;

iii) A_2 production, m = 0, by unnatural parity exchange, not interfering with π exchange [Z exchange [23]];

iv) A_2 production, m = 1, by B exchange.

We have parametrized the amplitudes corresponding to model (i) by

$$\bar{F}^{2,0}(\pi,B) = \bar{F}^{2,0}(\pi)\left\{1-ix_u \tan\left(\frac{\pi}{2}\left[t-\mu^2\right]\right)\exp\left(-i\frac{\pi}{2}\left[\alpha_B-\alpha_\pi\right]\right)\times\right.$$
$$\left.\times\exp\left(-\left[b_B-b_D\right]\left[\mu^2-t\right]\right)\times Z(F,A_2)\right\}, \qquad (10)$$

---

*) We have checked our absolute mass measurement on the K_S^0 mass which we find at m = 0.497 ± 0.0005 GeV, the FWHM of the distribution is 14 MeV. The error on the invariant $K_S^0K_S^0$ mass in the f region is estimated at ΔM = +7 MeV.

**) We use $\Gamma(A_2 \to \bar{K}K) = 4.7$ MeV [22] and $\Gamma(f \to K\bar{K}) = 4.1$ MeV (see Table 1) and therefore $\Gamma(A_2 \to KK)/\Gamma(f \to K\bar{K}) = 1.15$.

where

$$Z(f,A_2) = \frac{m_f^2 - i\, m_f\, \Gamma_f(M) - M^2}{m_{A_2}^2 - i\, m_{A_2}\, \Gamma_{A_2}(M) - M^2} ,$$

and

$$\alpha_B - \alpha_\pi = -0.25 .$$

Duality arguments[23] suggest that $|b_B - b_D|$ (the difference in the D-wave slopes of B exchange and π exchange) is small and that $x_u \simeq +1$. We have also estimated these two parameters from ρ_{00} $d\sigma/dt$ observed in $\pi^+ n \to A_2^0 p$ [18] and found $|x_u| \simeq 2.2$ and $b_D \simeq 5$ GeV^{-2}. Using Eq. (10) we have performed fits similar to 5.2.1 both with the values of b_D, x_u derived from duality[23] and from experiment[18]. Both fits were found to be unacceptable. A further fit with x_u being a free parameter resulted in $x_u = 0$. The reason for the rejection of the new term in Eq. (10) was found to be the t-dependence of the phase implied by Eq. (10), which phase is incompatible with the S-D interference of our data. Moreover, this type of f-A_2 interference does not result in such a shape of the f-A_2 peak that a larger f width is needed to fit the data. We have checked this point in a fit where the extra phase introduced by Eq. (10) was suppressed in order to make the model more sensitive to the f-A_2 interference.

The natural parity exchanges corresponding to the A_2 production amplitude (ii) give an additional term to $\overset{+}{F}{}^{2,1}$ [Eq. (1)] similar to the one in $\bar{F}^{2,0}(\pi,B)$, Eq. (10), i.e.

$$\overset{+}{F}{}^{2,1}_{+-}(\mathrm{cut},A_2,\rho) = F_D \left\{ -\frac{C}{2} \frac{d_{01}^2}{\sqrt{-t'}}\bigg|_{t=\mu^2} e^{-b_C(\mu^2-t)} + \eta\left[1 - i x_n \tan\left(\frac{\pi}{2}\alpha_{\rho,A_2}\right)\right] Z(f,A_2)\right] \times$$

$$\times (-t')\, e^{-i(\pi/2)(\alpha_{\rho,A_2}-\alpha_\pi)}\, e^{b_{\rho,A_2} t} \Big\} . \qquad (11)$$

We estimate from the results on f production in $\pi^- p \to \pi^+\pi^- n$ at 17.2 GeV/c [9] the following parameter values: $b_{\rho,A_2} = 2.5$ GeV^{-2}, $\eta = 2$ GeV^{-3}; and from the data on $\overset{+}{\rho}{}^{22}_{11}$ $d\sigma/dt$ in $\pi^+ n \to A_2^0 p$ [18]: $\eta x_n \simeq 4$ GeV^{-3} and $b_{\rho,A_2} \simeq 1$ GeV^{-2}. From duality, one predicts[23] again $x_n \simeq +1$. Since in the analogous case of ρ-ω production by natural parity exchange a larger value of x_n has been found[23], we may also expect $|x_n| > 1$ here.

In a fit using the amplitude of Eq. (11) we have set $b_{\rho,A_2} = 2.5$ GeV^{-2}, $x_n = 2$; η was a free parameter. This resulted in an improved fit (the logarithm of the likelihood increased by 8 to 9 units); we observe that the improvement is due to a better agreement of the model with the data in the moments $\langle Y_2^2 \rangle$, $\langle Y_4^0 \rangle$, and $\langle Y_4^2 \rangle$ in the region $0.2 < |t| < 0.5$ GeV^2. The best fit value of η depends on

the parameter $\alpha_{\rho,A_2} - \alpha_\pi$. Choosing $\alpha_{\rho,A_2} - \alpha_\pi = 0.5$ we find $\eta = 2.2 \pm 0.5$ GeV^{-3}, i.e. $\eta x_n = (4.4 \pm 1)$ GeV^{-3}. This compares well with the estimate deduced from the $\pi^+ n$ experiment[18]. Our data therefore are in agreement with this small component of A_2^0 produced by natural parity exchange.

As A_2^0 production by B exchange with m = 0, interfering with f production by π exchange, seems to be excluded by our data, we have also performed a fit mentioned under (iii), i.e. we have added incoherently unnatural parity exchange. In fact, unnatural parity exchange in $\pi^- p \to A_2^0 n$ with m = 0 can be either totally coherent or totally incoherent with the π exchange in $\pi^- p \to fn$, depending on the signature. While the B meson is a good candidate for such mesons with odd signature, the representative of the other class, e.g. the Z meson with $J^P I^G = 2^- 1^+$, has appeared so far only in theoretical papers[23]. For a fit we have used Eq. (10) and the values of the parameters given there. We have retained the t-dependence of Eq. (10) but removed from the expression of $d^3\sigma/(dtdMd\Omega)$ all interference terms containing x_u. We observe an improvement in the fit (the logarithm of the likelihood increases by 5.5 with respect to the fit 5.2.1 of Section 5). Moreover, m_f and Γ_f now tend to shift towards the values found in $\pi^- p \to \pi^+\pi^- n$ [7]: $\Delta m_f = -4$ MeV and $\Delta\Gamma_f = +10$ MeV. Our data therefore seem to support unnatural parity exchange not interfering with π exchange. This constitutes some evidence that at least part of the $\pi^+ n \to A_2^0 p$ cross-section is due to Z exchange.

The compatibility test, mentioned under (iv) of a m = 1 unnatural parity exchange amplitude for A_2 production is motivated by the anomaly in $\langle Y_4^1 \rangle$ in the 1.35 GeV region. A contribution to $\langle Y_4^1 \rangle$ implies interference of this amplitude with the dominant π-exchange amplitude and B exchange is therefore appropriate. For this model calculation we have replaced $\bar{F}^{2,1}(\text{cut})$ of Eq. (1) by

$$\bar{F}^{2,1}_{+-}(\text{cut,B}) = \bar{F}^{2,1}_{+-}(\text{cut}) \left[1 + y\, e^{i\psi}\, Z(f,A) \right], \qquad (12)$$

where y is an effective strength parameter of B exchange. From the experiment $\pi^+ n \to A_2^0 p$ [18] we estimate $y \simeq 0.4$. In a fit containing Eq. (12) we find $\psi = 140° \pm 15°$ which is consistent with B exchange. We have plotted the result of the fit in Fig. 4c as a dashed line. The effect of including Eq. (12) into the model is seen to go in the right direction as also witnessed by the increase of the logarithm of the likelihood by 8 units. Better fits to $\langle Y_4^1 \rangle$ can be obtained with larger values of y; however, discrepancies appear in $\langle Y_2^1 \rangle$ in this case.

6.6 The branching ratio $f \to K\bar{K}$

With Eq. (3) and the expression of the differential cross-section given in the Appendix we determine from our data the product of branching ratios $(\Gamma_f^\pi/\Gamma_f)\cdot(\Gamma_f^K/\Gamma_f)$; its value is given in Table 1. Using $x = \Gamma_f^\pi/\Gamma_f = 0.83 \pm 0.05$ [22]

we deduce

$$\Gamma_f^K/\Gamma_f^\pi = 0.029 \pm 0.006 \ ,$$

where the error is mainly due to the uncertainty on the cross-section normalization.

This branching ratio is, within errors, compatible with the world average compiled by the Particle Data Group[22]. A recent measurement of $\Gamma(f \to 4\pi)/\Gamma(f \to$ $\to$ all) gave $0.11 \pm {}^{0.02}_{0.03}$ [24] [under the assumption that the 4π decay goes mainly via $\rho\rho$]. An even higher value of the same quantity, 0.19 ± 0.06, has been found in an experiment on $\pi^+ n \to f\Delta^{++}$ [25]. These measurements indicate a near saturation of the inelasticity expected from $x = 0.83$ [22] by $f \to 4\pi$, in agreement with our comparatively low $K\bar{K}$ branching ratio.

An SU(3) estimate of this branching ratio, based on other, well-measured, $2^+ \to 0^-0^-$ decay rates, has resulted in $\Gamma_f^K/\Gamma_f^\pi = 0.04 \pm 0.015$ [17]. Our result is also compatible with this value.

6.7 The decay rate $\Gamma(f^* \to \pi\pi)$

This subject has been discussed in a recent letter[26]. We mention it here for completeness and for presenting an updated SU(3) fit for all $2^+ \to 0^-0^-$ decay rates.

As in the case of the f, we can determine from our data the ratio $(\Gamma_{f'}^\pi/\Gamma_{f'}) \cdot (\Gamma_{f'}^K/\Gamma_{f'})$. Conversely to the case of the f, $\Gamma_{f'}^\pi$ is here the small decay rate (the production channel). We estimate a conservative upper limit (see Ref. 26) by assuming the total D-wave at the f′ mass, as obtained in the mass-independent fit 5.1 to be due to f′ production. Comparing $|D|^2$ of the f peak with $|D|^2$ of the f′ mass we find (see Fig. 10b) for the ratio R:

$$R = \left(\frac{\Gamma_{f'}^\pi \cdot \Gamma_{f'}^K}{\Gamma_{f'}^2}\right)\left(\frac{\Gamma_f^\pi \cdot \Gamma_f^K}{\Gamma_f^2}\right)^{-1} \leq \frac{1}{3} \ . \qquad (13a)$$

This result is independent of our cross-section normalization and it is also model-independent except for the assumption that f and f′ have the same production mechanism.

For a numerical estimate of f′ production we have added to the D-wave amplitude Eq. (3) a Breit-Wigner amplitude for the f′ *). For a fit to the data we found an amplitude of a sign opposite to that of the f and of a strength given by

$$R = \left(0.04 \ {}^{+0.05}_{-0.03}\right) \ . \qquad (13b)$$

*) In order to make the fit independent of the S-wave phase, which is unknown in this region, we have retained the D-wave phase of Eq. (3) in the expressions of S-D interference.

In the fits described below, we have taken R = 0.04 as the central value and R = 1/3 [Eq. (13a)] as its two standard deviation upper limit.

We have used this result to determine a new value of the mixing angle in the 2^+ nonet in a fit of all available $2^+ \to 0^-0^-$ decay rates to the SU(3) relations. Further experimental inputs to this fit were $\Gamma(f \to K\bar{K})$ (see Section 6.6), a recently published upper limit of $\Gamma(f \to \eta\eta)$ [27], and the decay rates and upper limits given by the Particle Data Group[22]. We have also taken into account the mixing angle of the pseudoscalar nonet. This leads to four terms in the amplitudes for $2^+ \to 0^-0^-$ [a(T → PP)] which we defined symbolically by

$$a(T \to PP) = A \cdot Tr(T\{P,P\}) + B \cdot TrT \cdot Tr(PP)$$
$$+ C \cdot TrP \cdot Tr(TP) + D \cdot TrT \cdot TrP \cdot TrP \ .$$

The 3 × 3 matrices T,P describe the members of the tensor and pseudoscalar nonet, respectively[28]. In particular, f and f′ are in this notation

$$|f\rangle = \frac{1}{\sqrt{2}} \cos(\theta_C - \theta_2) \ |T_1^1 + T_2^2\rangle + \sin(\theta_C - \theta_2) \ |T_3^3\rangle$$

$$|f'\rangle = \frac{1}{\sqrt{2}} \sin(\theta_C - \theta_2) \ |T_1^1 + T_2^2\rangle - \cos(\theta_C - \theta_2) \ |T_3^3\rangle$$

where θ_C is the ideal mixing angle ($\tan\theta_C = \sqrt{1/2}$). The states η and η′ have a similar form in terms of the matrix P and the mixing angle θ_0. The first term of the decay amplitude, with the coefficient A, obeys the Zweig rule[29]; all other terms violate it. We have used the usual barrier penetration and phase-space factor q^5/M, where M is the mass of the decaying particles and q the c.m.s. momentum of its decay products.

The input to the fit of the partial widths and their best fit values are shown in Table 3. The best fit values of the f and K^{**} decay rates are smaller than the experimental ones, while the converse is true for the A_2 decay rates. In order to be more independent of the total widths, we have performed a second fit with the error on the total widths of A_2, K^{**}, and f′, increased by a factor of 2, and in which branching fractions were fitted whenever possible. The result of this fit is also shown in Table 3.

A fit of all six parameters of the decay amplitudes (A, B, C, D, θ_2, θ_0) results in large errors on C, D, and θ_0 which involve the singlet of the pseudoscalar nonet. For the other parameters we find A = 0.795 ± 0.031, B = −0.018 ± 0.03, and $\theta_2 = (36.3 \pm 1.9)°$. The amplitude violating the Zweig rule turns out to be compatible with zero and at most a few percent of the total $2^+ \to 0^-0^-$ amplitude. When we set B = C = D = 0, we find $\theta_2 = (36.2 \pm 1)°$ and $\theta_0 = (-10.6 \pm 3.3)°$ with

$\chi^2 = 3$ for 7 degrees of freedom (see Table 3). The tensor nonet mixing angle θ_2 is compatible with the ideal angle $\theta_C = 35.26°$. From the observation made above, that a fit of an f′ amplitude to our data results in its sign being opposite to the f amplitude we would expect $\theta_2 < \theta_C$. The fit to the decay rates depends linearly on θ_2 only in the expression of $\Gamma(f \to K\bar{K})$ in which increasing θ_2 leads to a decreasing width, i.e. $\theta_2 < \theta_C$ predicts a $\Gamma(f \to K\bar{K})$ larger than the experimental input.

The value of the pseudoscalar mixing angle $\theta_0 = (-10.6 \pm 3.3)°$ is in good agreement with $|\theta_0|$ derived from the quadratic Gell-Mann/Okubo mass formula[17] and with $\theta_0 \simeq -10°$ found in an analysis of pseudoscalar electromagnetic decays[30].

Acknowledgements

We gratefully acknowledge the help of Drs. R. Frosch and E. Polgàr in the initial stages of the experiment and of Mrs. J. Chappuis and A. Mazzari who carefully remeasured the events not found by the automatic machine.

REFERENCES

1) P. Astbury, G. Finocchiaro, A. Michelini, D. Websdale, C.H. West, W. Beusch, B. Gobbi, M. Pepin, E. Polgàr and M. Pouchon, Nuclear Instrum. Methods, 46 (1967) 61.

2) W. Beusch, A. Michelini, D. Websdale, W.E. Fischer, R. Frosch, P. Mühlemann, M. Pepin, E. Polgàr, J. Codling and M.G. Green, Nuclear Phys. B19 (1970) 546.

3) E. Etim, G. Pancheri and B. Touschek, Nuovo Cimento 51B (1967) 276.

4) G. Grayer, B. Hyams, C. Jones, P. Schlein, W. Blum, H. Dietl, W. Koch, H. Lippmann, E. Lorenz, G. Lütjens, W. Männer, J. Meissburger, U. Stierlin and P. Weilhammer, Phys. Letters 34B (1971) 333.

5) W. Beusch, W.E. Fischer, B. Gobbi, M. Pepin, E. Polgàr, P. Astbury, G. Brautti, G. Finocchiaro, J.C. Lassalle, A. Michelini, K.M. Terwilliger, D. Websdale and C.H. West, Phys. Letters 25B (1967) 357.

6) W. Beusch *in* Experimental meson spectroscopy (eds. C. Baltay and A.H. Rosenfeld) (Columbia University Press, New York and London, 1970).

7) P. Estabrooks and A.D. Martin; G. Grayer, B. Hyams, C. Jones, P. Weilhammer; W. Blum, H. Dietl, W. Koch, E. Lorenz, G. Lütjens, W. Männer, J. Meissburger and U. Stierlin *in* Proc. Internat. Conf. on ππ Scattering, Tallahasse, 1973 (American Institute of Physics, New York, 1973), p. 37.

8) M. Ross, F.S. Henyey and G.L. Kane, Nuclear Phys. B23 (1970) 269.

9) A.D. Martin *in* Proc. 4th Internat. Symposium on Multiparticle Hadron Dynamics, Pavia, 1973 (eds. F. Duimio, A. Giovannini and S. Ratti) (INFN, Pavia, 1973), p. 203.

10) P.K. Williams, Phys. Rev. D 1 (1970) 1312.

11) G. Grayer, B. Hyams, C. Jones, P. Schlein, P. Weilhammer, W. Blum, H. Dietl, W. Koch, E. Lorenz, G. Lütjens, W. Männer, J. Meissburger, W. Ochs and U. Stierlin, Nuclear Phys. B64 (1973), 134 and Nuclear Phys. B75 (1974) 189.

12) G. Grayer, B. Hyams, C. Jones, P. Schlein, P. Weilhammer, W. Blum, H. Dietl, W. Koch, D. Lorenz, G. Lütjens, W. Männer, J. Meissburger, W. Ochs and U. Stierlin *in* Proc. Internat. Conf. on ππ Scattering, Tallahasse, 1973 (American Institute of Physics, New York, 1973), p. 117.

13) A.J. Pawlicki, D.S. Ayres, R. Diebold, A.F. Greene, S.L. Kramer and A.B. Wicklund, preprint ANL/HEP 75-09, submitted to Phys. Rev.

14) S.D. Protopopescu, M. Alston-Garnjost, A. Barbaro-Galtieri, S.N. Flatté, J.H. Friedman, T.A. Lasinski, G.R. Lynch, M.S. Rabin and F.T. Solmitz, Phys. Rev. D 7 (1973) 1279.

15) B. Hyams, C. Jones, P. Weilhammer, W. Blum, H. Dietl, G. Grayer, W. Koch, E. Lorenz, G. Lütjens, W. Männer, J. Meissburger, W. Ochs and U. Stierlin, Nuclear Phys. B100 (1975) 205.

16) P. Estabrooks and A.D. Martin, Nuclear Phys. B95 (1975) 322.

17) N.P. Samios, M. Goldberg and B.T. Meadows, Rev. Mod. Phys. 46 (1974) 49.

18) M.J. Emms, G.T. Jones, J.B. Kinson, B.J. Stacey, M.F. Votruba, P.L. Woodworth, I.G. Bell, M. Dale, D. Evans, M.J. Major, J.A. Charlesworth, D.J. Crennell and R.L. Sekulin, Phys. Letters 58B (1975) 117.

19) J.T. Carroll, M.W. Firebaugh, A. Garfinkel, R. Morse, B.Y. Oh, W. Robertson, W.D. Walker, J.A.J. Matthews, J.D. Prentice, T.F. Johnston and T.S. Yoon, Phys. Rev. Letters 25 (1970) 1393.

20) Yu.M. Antipov, G. Ascoli, R. Busnello, M.N. Kienzle-Focacci, W. Kienzle, R. Klanner, A.A. Lebedev, P. Lecomte, V. Roinishvili, A. Weitsch and F.A. Yotch, Nuclear Phys. B63 (1973) 153.

21) H.A. Gordon, M. Habibi, I. Stumer and Kwan-Wu Lai, Phys. Rev. Letters 33 (1974) 603.

22) Particle Data Group, Phys. Letters 50B (1974) 1.

23) A.C. Irving and C. Michael, Nuclear Phys. B82 (1974) 282.

24) J. Louie, J. Alitti, B. Gandois, J. Mallet, V. Chaloupka, A. Ferrando, M.J. Losty, L. Montanet, E. Paul, D. Yaffe and A. Zieminski, Phys. Letters 48B (1974) 385.

25) Y. Eisenberg, A. Engler, B. Haber, U. Karshon, G. Mikenberg, S. Pitluck, E.E. Ronat, A. Shapira and G. Yekuteli, Phys. Letters 52B (1974) 259.

26) W. Beusch, A. Birman, D. Websdale and W. Wetzel, Phys. Letters 60B (1975) 205.

27) M.J. Emms, J.B. Kinson, B.J. Stacey, M.F. Votruba, P.L. Woodworth, I.G. Bell, M. Dale, J.V. Major, J.A. Charlesworth, D.J. Crennell and R.L. Sekulin, Nuclear Phys. B96 (1975) 155.

28) S. Okubo, Phys. Letters 5 (1963) 165.

29) G. Zweig, CERN TH-401 and TH.412, unpublished.

30) A. Bramon and N. Greco, Phys. Letters 48B (1974) 137.

APPENDIX

A) Density matrix elements

Writing the $K\bar{K}$ angular distribution $W(\Omega)$ in terms of the $K\bar{K}$ density matrix elements,

$$W(\Omega) = \sum_{\substack{\ell_1,\ell_2 \\ m_1,m_2}} Y^{m_2}_{\ell_2}(\Omega)\ \rho^{\ell_2\ell_1}_{m_2m_1}\ \overline{Y^{m_1}_{\ell_1}(\Omega)}$$

leads to the following expressions for the moments $\langle Y^M_L \rangle$:

$$\langle Y^0_0 \rangle = \frac{1}{\sqrt{4\pi}} \left\{ \rho^{00}_{00} + \rho^{22}_{00} + 2\,\rho^{22}_{11} + 2\,\rho^{22}_{22} \right\}$$

$$\langle Y^0_2 \rangle = \frac{1}{\sqrt{4\pi}} \left\{ 2\ \mathrm{Re}\ \rho^{20}_{00} + \frac{2}{7}\sqrt{5}\,\rho^{22}_{00} + \frac{2}{7}\sqrt{5}\,\rho^{22}_{11} - \frac{4}{7}\sqrt{5}\,\rho^{22}_{22} \right\}$$

$$\langle Y^0_4 \rangle = \frac{1}{\sqrt{4\pi}} \left\{ \frac{6}{7}\,\rho^{22}_{00} - \frac{8}{7}\,\rho^{22}_{11} + \frac{2}{7}\,\rho^{22}_{22} \right\}$$

$$\langle \mathrm{Re}\ Y^1_2 \rangle = \frac{1}{\sqrt{4\pi}} \left\{ 2\ \mathrm{Re}\ \rho^{20}_{10} + \frac{2}{7}\sqrt{5}\ \mathrm{Re}\ \rho^{22}_{10} + \frac{2}{7}\sqrt{30}\ \mathrm{Re}\ \rho^{22}_{21} \right\}$$

$$\langle \mathrm{Re}\ Y^1_4 \rangle = \frac{1}{\sqrt{4\pi}} \left\{ \frac{2}{7}\sqrt{30}\ \mathrm{Re}\ \rho^{22}_{10} - \frac{2}{7}\sqrt{5}\ \mathrm{Re}\ \rho^{22}_{21} \right\}$$

$$\langle \mathrm{Re}\ Y^2_2 \rangle = \frac{1}{\sqrt{4\pi}} \left\{ 2\ \mathrm{Re}\ \rho^{20}_{20} - \frac{4}{7}\sqrt{5}\ \mathrm{Re}\ \rho^{22}_{20} - \frac{1}{7}\sqrt{30}\ \mathrm{Re}\ \rho^{22}_{1\,-1} \right\}$$

$$\langle \mathrm{Re}\ Y^2_4 \rangle = \frac{1}{\sqrt{4\pi}} \left\{ \frac{2}{7}\sqrt{15}\ \mathrm{Re}\ \rho^{22}_{20} - \frac{2}{7}\sqrt{10}\ \mathrm{Re}\ \rho^{22}_{1\,-1} \right\}$$

$$\langle \mathrm{Re}\ Y^3_4 \rangle = -\frac{1}{\sqrt{4\pi}}\ 2\sqrt{\frac{5}{7}}\ \rho^{22}_{2\,-1}$$

$$\langle \mathrm{Re}\ Y^4_4 \rangle = \frac{1}{\sqrt{4\pi}}\sqrt{\frac{10}{7}}\ \rho^{22}_{2\,-2}$$

B) Crossing angle χ

$$\cos\chi = \frac{\left[s + M^2(K\bar{K}) - m_n^2\right]\left[t + M^2(K\bar{K}) - \mu^2\right] - 2M^2(K\bar{K})\cdot\Delta}{\lambda_{\frac{1}{2}}\left[s, M^2(K\bar{K}), m_n^2\right]\ \lambda_{\frac{1}{2}}\left[t, M^2(K\bar{K}),\ \mu^2\right]}$$

$$\sin\chi \geq 0$$

$$\Delta = M^2(K\bar{K}) - \mu^2 + m_p^2 - m_n^2$$

$$\lambda_{\frac{1}{2}}\ (x_1,\ x_2,\ x_3) = \left[x_1^2 + x_2^2 + x_3^2 - 2x_1x_2 - 2x_1x_3 - 2x_2x_3\right]^{\frac{1}{2}}$$

C) Normalization

$$\frac{d^3\sigma(K^0\bar{K}^0,\ \ell \text{ even})}{dtdMd\Omega} = \frac{1}{(4\pi)^4}\,\frac{q_{K\bar{K}}}{4P^2_{lab}\ m_p^2}\,\frac{1}{2}\sum_{\lambda_f,\lambda_i}\left|\sum_{\ell,m} F^{\ell,m}_{\lambda_f\lambda_i}\ Y^m_\ell(\Omega)\right|^2$$

$$F_S = \sqrt{2}\,\sqrt{\frac{g^2}{4\pi}}\,\frac{(4\pi)^2 M_{KK}}{(q_{\pi\pi}\ q_{KK})^{\frac{1}{2}}}\,\sqrt{\frac{1}{3}}\ S$$

$$F_D = \sqrt{2}\,\sqrt{\frac{g^2}{4\pi}}\,\frac{(4\pi)^2 M_{KK}}{(q_{\pi\pi}\ q_{KK})^{\frac{1}{2}}}\,\sqrt{\frac{1}{3}}\ \sqrt{5}\ D$$

$$|S|^2 \le 1,\quad |D|^2 \le 1 \text{ by unitarity}$$

D) Energy dependence of partial widths

$$D_2(x) = 9 + 3x^2 + x^4,\qquad R_f = 3.5\ (\text{GeV})^{-1}$$

$$\Gamma^\pi_f(M) = \Gamma^\pi_f\left(\frac{q_{\pi\pi}(M)}{q_{\pi\pi,f}}\right)^5 \frac{D_2(q_{\pi\pi,f}\ R_f)}{D_2(q_{\pi\pi}(M)\ R_f)}$$

$$\Gamma^K_f(M) = \Gamma^K_f\left(\frac{q_{KK}(M)}{q_{KK,f}}\right)^5 \frac{D_2(q_{KK,f}\ R_f)}{D_2(q_{KK}(M)\ R_f)}$$

The total widths $\Gamma_f(M)$ and $\Gamma_{A_2}(M)$ have the mass dependence of the $\pi\pi$ and $\rho\pi$ channel, respectively.

E) Moment combinations M_1, M_2, M_3

$$M_1 = \sqrt{4\pi}\left\{\frac{2}{5}\langle Y^0_0\rangle + \frac{7}{10}\langle Y^0_4\rangle\right\}$$
$$= \rho^{22}_{00} + \frac{2}{5}\rho^{00}_{00} + \rho^{22}_{22}$$

$$M_2 = \sqrt{4\pi}\left\{\frac{3}{10}\langle Y^0_0\rangle - \frac{7}{20}\langle Y^0_4\rangle\right\}$$
$$= \rho^{22}_{11} + \frac{3}{10}\rho^{00}_{00} + \frac{1}{2}\rho^{22}_{22}$$

$$M_3 = \sqrt{4\pi}\left\{\frac{1}{2\sqrt{5}}\langle Y^0_0\rangle - \frac{1}{2}\langle Y^0_2\rangle + \frac{1}{4\sqrt{5}}\langle Y^0_4\rangle\right\}$$
$$= -\ \text{Re}\ \rho^{20}_{00} + \frac{1}{2\sqrt{5}}\rho^{00}_{00} + \frac{\sqrt{5}}{2}\rho^{22}_{22}$$

These combinations have the property that the density matrix elements ρ^{20}_{00}, ρ^{22}_{00}, and ρ^{22}_{11} become separated. The moment M_2 is very suitable for the study of the S-wave cross-section at small t.

Table 1

Result of the mass-dependent fit 5.2.1
in the resonance region

m_f	1282 ± 5 MeV
Γ_f	159 ± 10 MeV
$(\Gamma_f^\pi/\Gamma_f)\cdot(\Gamma_f^K/\Gamma_f)$	0.020 ± 0.004
S_0^2	0.29 ± 0.03
m_S	1494 ± 6 MeV
Γ_S	71 ± 15 MeV
ε	0.0 ± 0.05
ϕ_1	142° ± 8°
ϕ_2	208° ± 18°
C	0.48 ± 0.05
b_S	1.57 ± 0.2 GeV^{-2}
b_D	0.31 ± 0.15 GeV^{-2}
b_C	0.33 ± 0.35 GeV^{-2}

Table 2

Result of the mass-dependent fit 5.2.2
in the threshold region

$\|a\|$	6.32 ± 0.6 GeV^{-1}
Im a	1.36 ± 0.15 GeV^{-1}
ϕ_S^0	255° ± 15°
b_S	1.7 ± 0.15 GeV^{-2}
$(\Gamma_f^\pi/\Gamma_f)\cdot(\Gamma_f^K/\Gamma_f)$	0.030 ± 0.01
C	0.7 ± 0.07

Table 3

SU(3) fit to the $(J^P)\ 2^+ \to 0^-0^-$ decays. The decay rates are given in GeV units. Best fit a): Input values from PDG table Ref. 22, from Ref. 27 and from this work; the last entry is the product of $f' \to \pi\pi$ and $f' \to K\bar{K}$ decay rates (symolically indicated as 9·10). Best fit b): enlarged errors on total decay rates and use of ratios as indicated by the decay rate code numbers.

Decay rate		Input to fit		Best fit a)		Input to fit		Best fit b)	
Code		Code	Value	Code	Value	Code	Value	Code	Value
1	$f \to \pi\pi$	1	0.141 ± 0.026	1	0.105	1	0.141 ± 0.026	1	0.120
2	$f \to K\bar{K}$	2	0.0041 ± 0.0012	2	0.0036	2/1	0.029 ± 0.006	2	0.0040
3	$f \to \eta\eta$	3	0 ± 0.0012	3	0.0003	3/1	0 ± 0.0036	3	0.0004
4	$A_2 \to \eta\pi$	4	0.0152 ± 0.002	4	0.0154	4	0.0152 ± 0.0035	4	0.0182
5	$A_2 \to K\bar{K}$	5	0.0047 ± 0.0005	5	0.0054	5/4	0.309 ± 0.046	5	0.0061
6	$A_2 \to \eta'\pi$	6	0 ± 0.0005	6	0.0006	6/4	0 ± 0.067	6	0.0007
7	$K^{**} \to K\pi$	7	0.055 ± 0.006	7	0.046	7	0.055 ± 0.012	7	0.052
8	$K^{**} \to K\eta$	8	0.002 ± 0.002	8	0.0004	8	0.002 ± 0.0025	8	0.00036
9	$f' \to \pi\pi$	9·10	$(14 \pm 70)\times10^{-6}$	9	0.0002	9+10+11	0.05 ± 0.02	9	0.00007
10	$f' \to K\bar{K}$			10	0.040	$\frac{9\cdot10}{(9+10+11)^2}$	0.0008 ± 0.0029	10	0.046
11	$f' \to \eta\eta$			11	0.0065			11	0.0069
		$\theta_0 = (-9.6 \pm 4.1)°$, $\theta_2 = (35.9 \pm 2.1)°$ χ^2/d.o.f. = 8/6				$\theta_0 = (-10.6 \pm 3.3)°$, $\theta_2 = (36.2 \pm 1)°$ χ^2/d.o.f. = 3/7			

Figure captions

Fig. 1 : Unnormalized moments $\langle Y_0^0 \rangle$: a) for $|t| \leq 0.2$ GeV^2, and b) for $0.2 \leq |t| \leq 0.5$ GeV^2. The ordinates are in units of events per 10 MeV $\left[\langle Y_0^0 \rangle = (1/\sqrt{4\pi}) \cdot (dN/dM)\right]$. The histogram refers to the data without weight; note the change of scale in the ordinate. The solid and dotted curves are the results of fits 5.2.1 and 5.2.2, respectively. These fits are discussed in the text.

Fig. 2 : The weight used for correcting the acceptance as a function of t and of cos θ. The mass intervals (in GeV) are: histogram a, $M < 1.2$; b, $1.2 < M < 1.4$; and c, $1.4 < M < 1.6$.

Fig. 3 : Unnormalized moments $\langle Y_2^0 \rangle$ and $\langle Y_2^1 \rangle$ for $|t| \leq 0.2$ (a,c) and $0.2 \leq |t| \leq 0.5$ GeV^2 (b,d). The ordinates are in units of weighted events per 10 MeV as explained in the Appendix. The solid and dotted curves are the results of fits 5.2.1 and 5.2.2, respectively (see text). The dashed line in $\langle Y_2^1 \rangle$ is discussed in Section 6.5.

Fig. 4 : Unnormalized moments $\langle Y_4^0 \rangle$ and $\langle Y_4^1 \rangle$ (see Fig. 3).

Fig. 5 : Unnormalized moments $\langle Y_2^2 \rangle$ and $\langle Y_4^2 \rangle$ (see Fig. 3).

Fig. 6 : Unnormalized moments $\langle Y_4^3 \rangle$ and $\langle Y_4^4 \rangle$ (see Fig. 3).

Fig. 7 : Unnormalized moments $\langle Y_6^0 \rangle$, $\langle Y_6^1 \rangle$, $\langle Y_8^0 \rangle$, and $\langle Y_8^1 \rangle$ for $|t| \leq 0.2$ GeV^2 (see Fig. 3).

Fig. 8 : t-dependence of $(d\sigma/dt')(\mu^2-t)^2$ at threshold (top) and in the resonance region (bottom). M is the $K\bar{K}$ mass in GeV; $q_{\pi\pi}$ is the pion momentum in the c.m.s. of $K\bar{K}$. The ordinate is in arbitrary units.

Fig. 9 : Energy dependence of $\sigma(\pi^- p \to K_S^0 K_S^0 n)$ derived from this and previous[4,5] experiments. The differential cross-section has been integrated over $0 \leq |t| \leq 0.5$ GeV^2 and over the mass bins indicated. The dashed lines indicate the p_{lab}^{-2} dependence.

Fig. 10 : Results of fitting the model to the data: magnitude and relative phase of S- and D-wave ($|S|^2$, $|D|^2$, $\phi_S - \phi_D$), cut strength parameter (C) and slope of S- and D-wave (b_S, b_D). The points are the result of a mass-independent fit (see Section 5.1). The solid and dotted lines refer to the mass-dependent fit in the resonance and in the threshold region, respectively (discussed in Section 5 under 5.2.1 and 5.2.2).

Fig. 11 : Momentum transfer dependence of the moment combinations M1, M2, M3 defined in the Appendix. The full curves are the result of fit 5.2.1; the dashed curve for M1, $1.27 \leq M(K\bar{K}) \leq 1.37$ GeV, indicates the effect of A_2 production (see text, Section 6.5).

Fig. 12 : Momentum transfer distribution in the threshold region. The curves are the result of the fit described in Section 5.2.2.

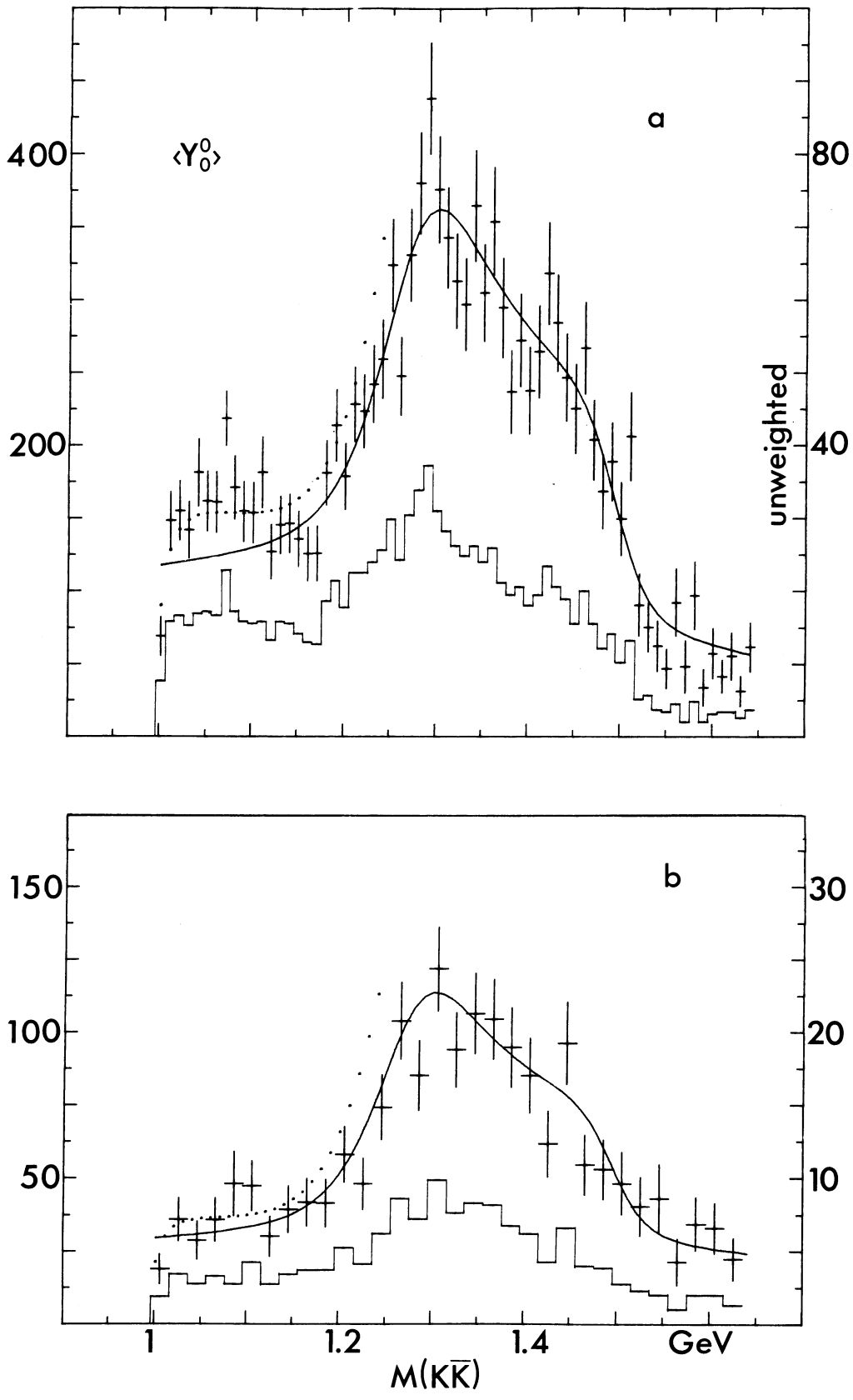
a
$\langle Y_0^0 \rangle$
400
200
80
40
unweighted
b
150
100
50
30
20
10
1
1.2
1.4
GeV
M(KK̄)

Fig. 1

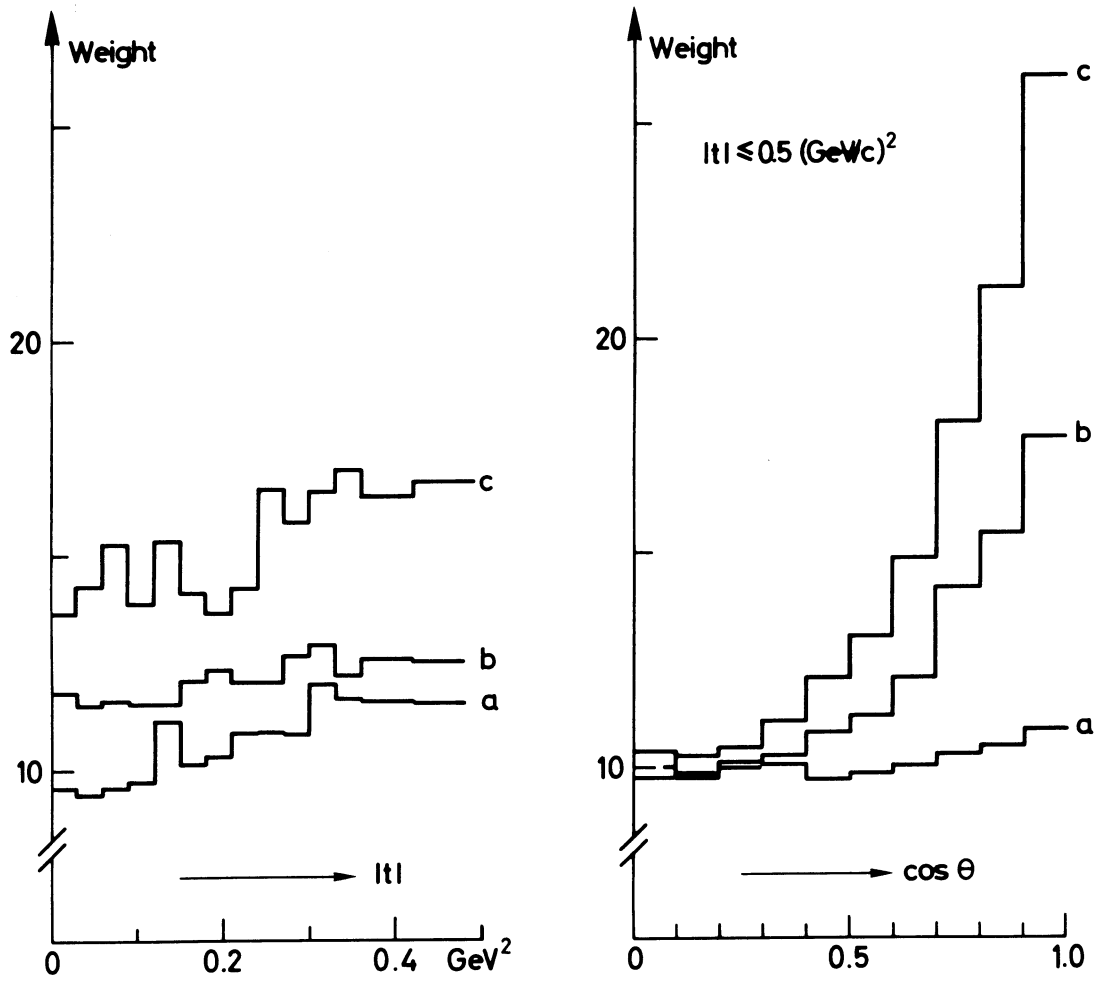
Weight
20
10
c
b
a
|t|
0
0.2
0.4
GeV²
Weight
|t| ≤ 0.5 (GeV/c)²
20
10
c
b
a
cos θ
0
0.5
1.0

Fig. 2

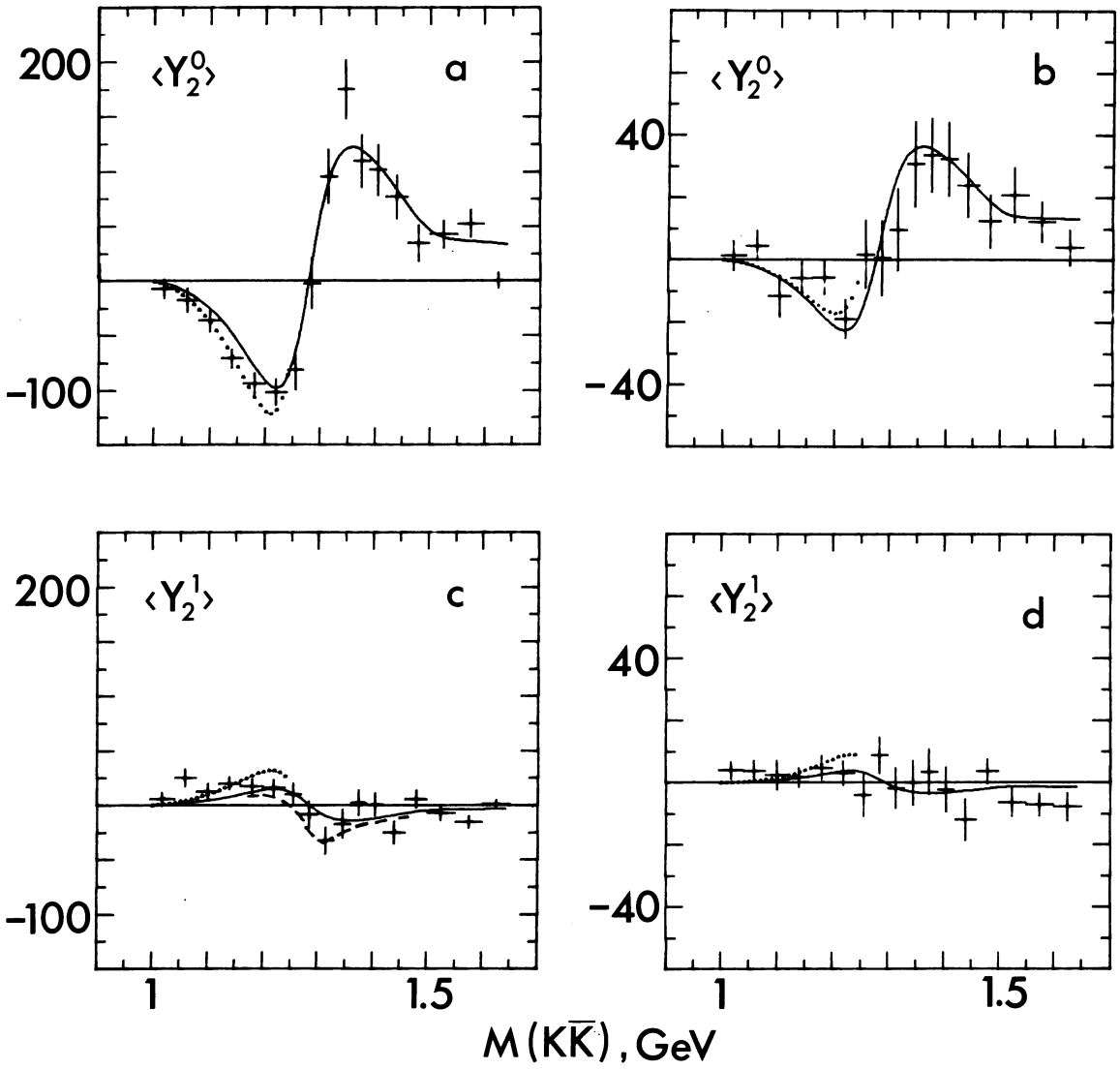

Fig. 3

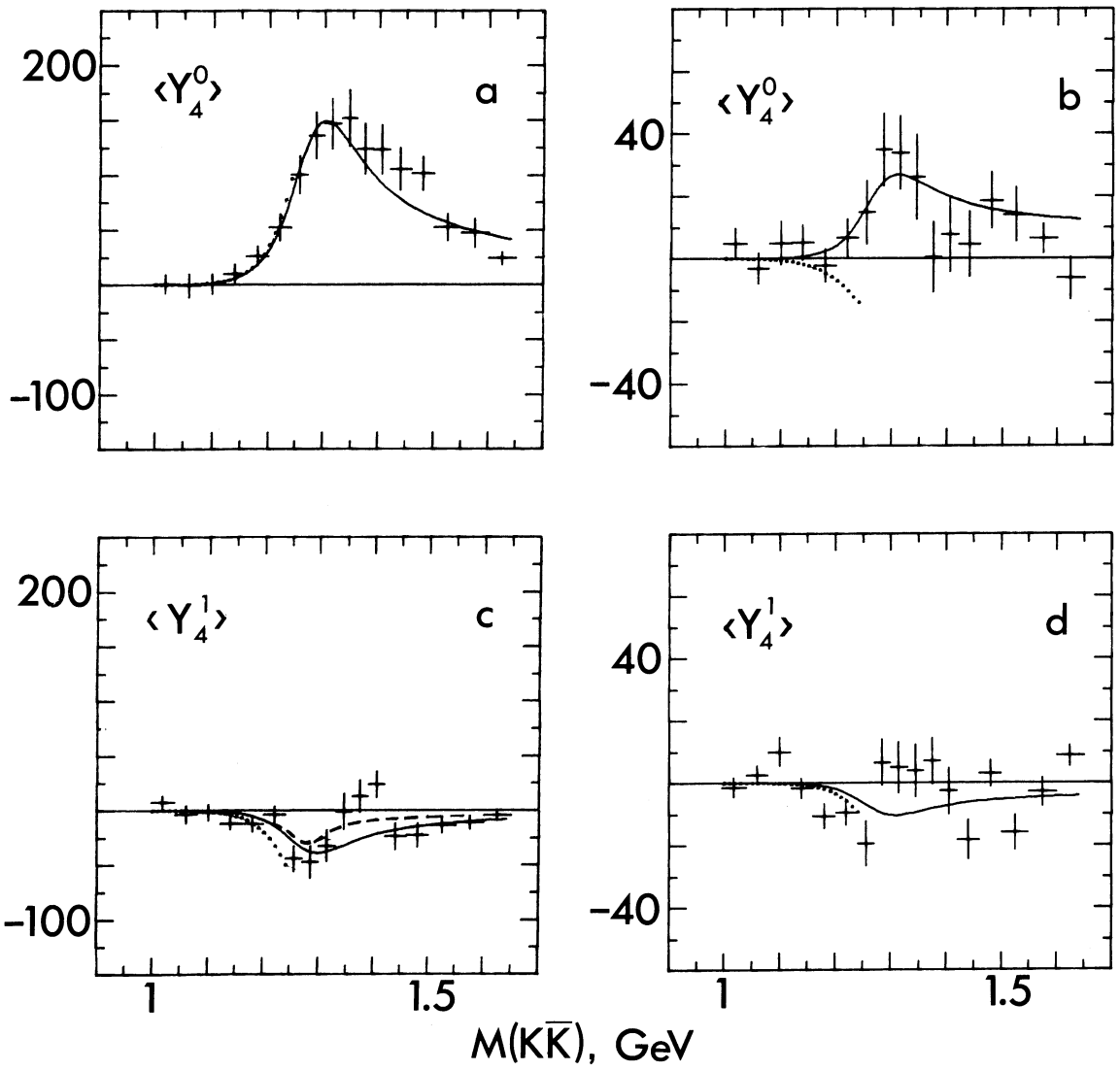
200
-100
$\langle Y_4^0 \rangle$
a
40
-40
$\langle Y_4^0 \rangle$
b
200
-100
$\langle Y_4^1 \rangle$
c
40
-40
$\langle Y_4^1 \rangle$
d
1
1.5
1
1.5
M(KK̄), GeV

Fig. 4

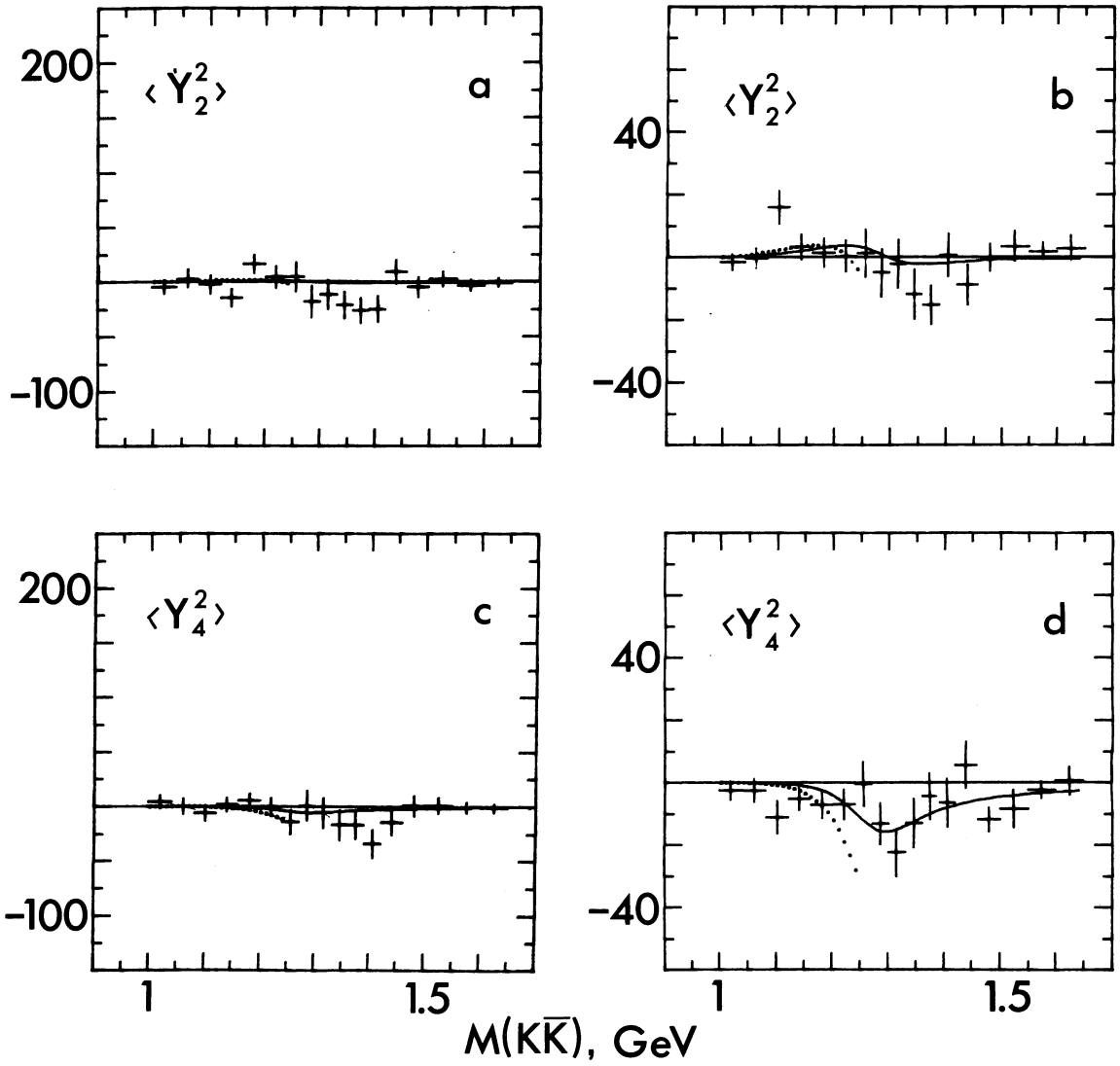
200
-100
$\langle Y_2^2 \rangle$
a
40
-40
$\langle Y_2^2 \rangle$
b
200
-100
$\langle Y_4^2 \rangle$
c
40
-40
$\langle Y_4^2 \rangle$
d
1
1.5
1
1.5
M(KK̄), GeV

Fig. 5

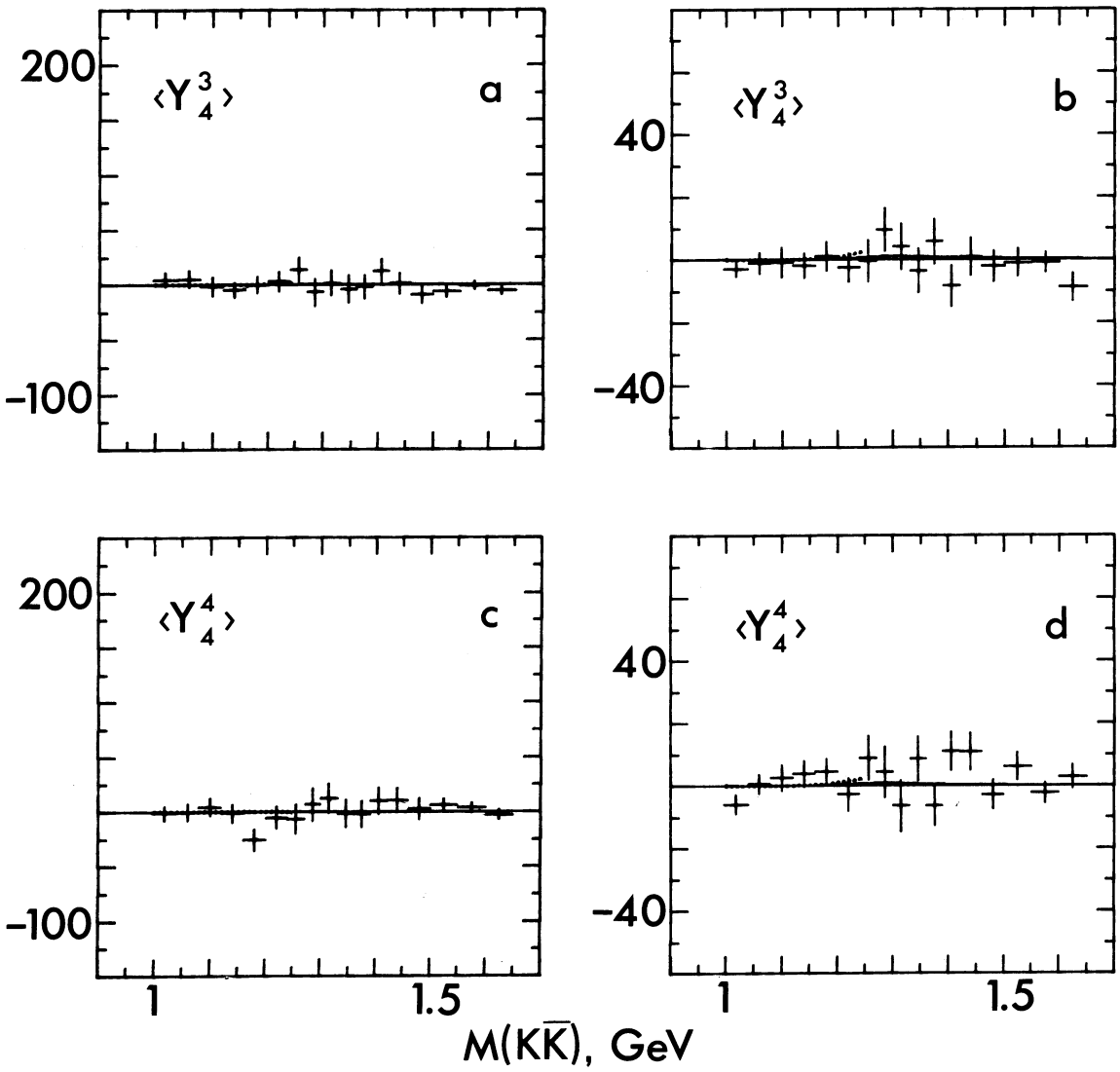
200
-100
$\langle Y_4^3 \rangle$
a
40
-40
$\langle Y_4^3 \rangle$
b
200
-100
$\langle Y_4^4 \rangle$
c
40
-40
$\langle Y_4^4 \rangle$
d
1
1.5
1
1.5
M(KK̄), GeV

Fig. 6

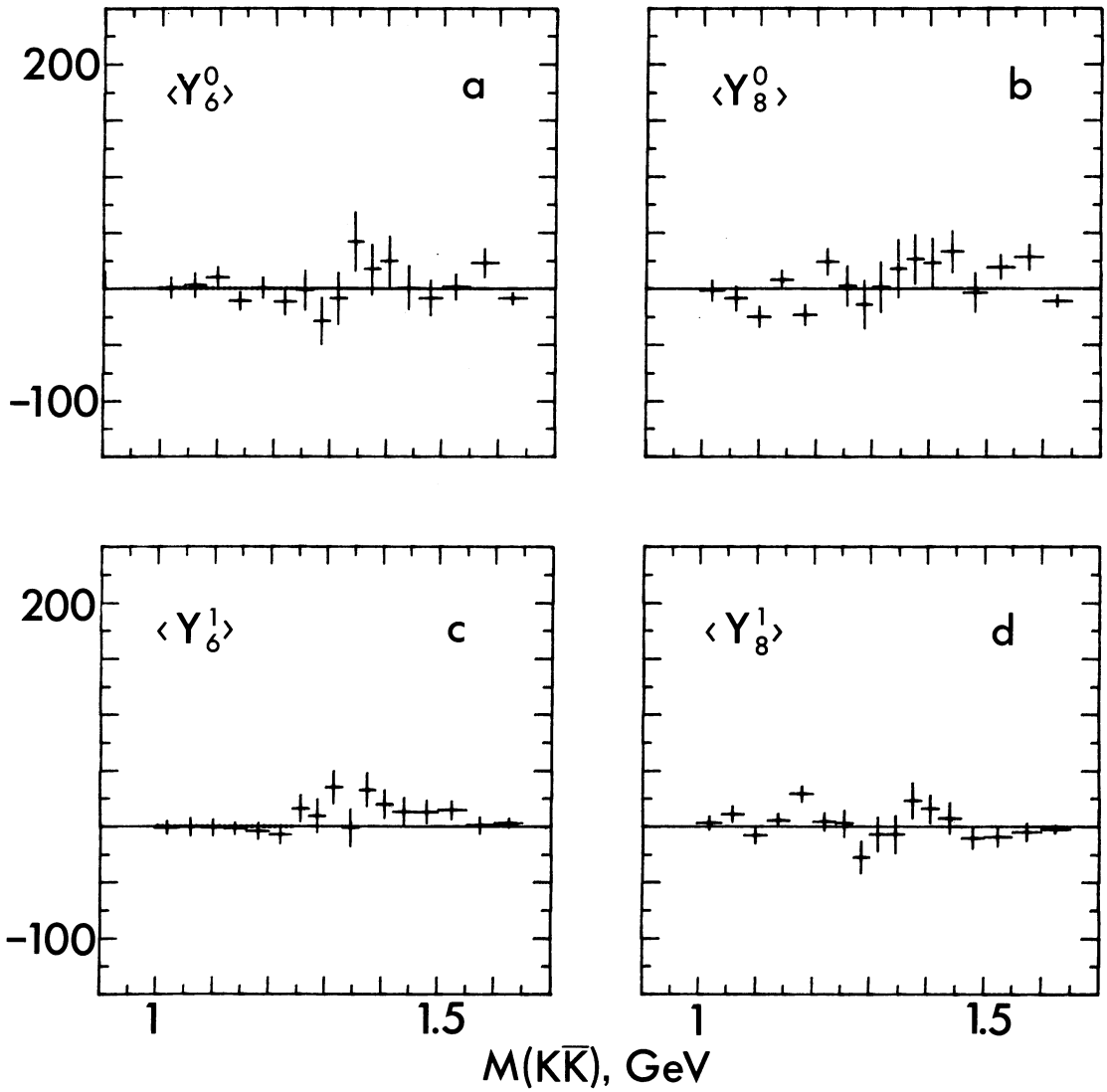
200
-100
$\langle Y_6^0 \rangle$
a
$\langle Y_8^0 \rangle$
b
200
-100
$\langle Y_6^1 \rangle$
c
$\langle Y_8^1 \rangle$
d
1
1.5
1
1.5
M(K$\bar{K}$), GeV

Fig. 7

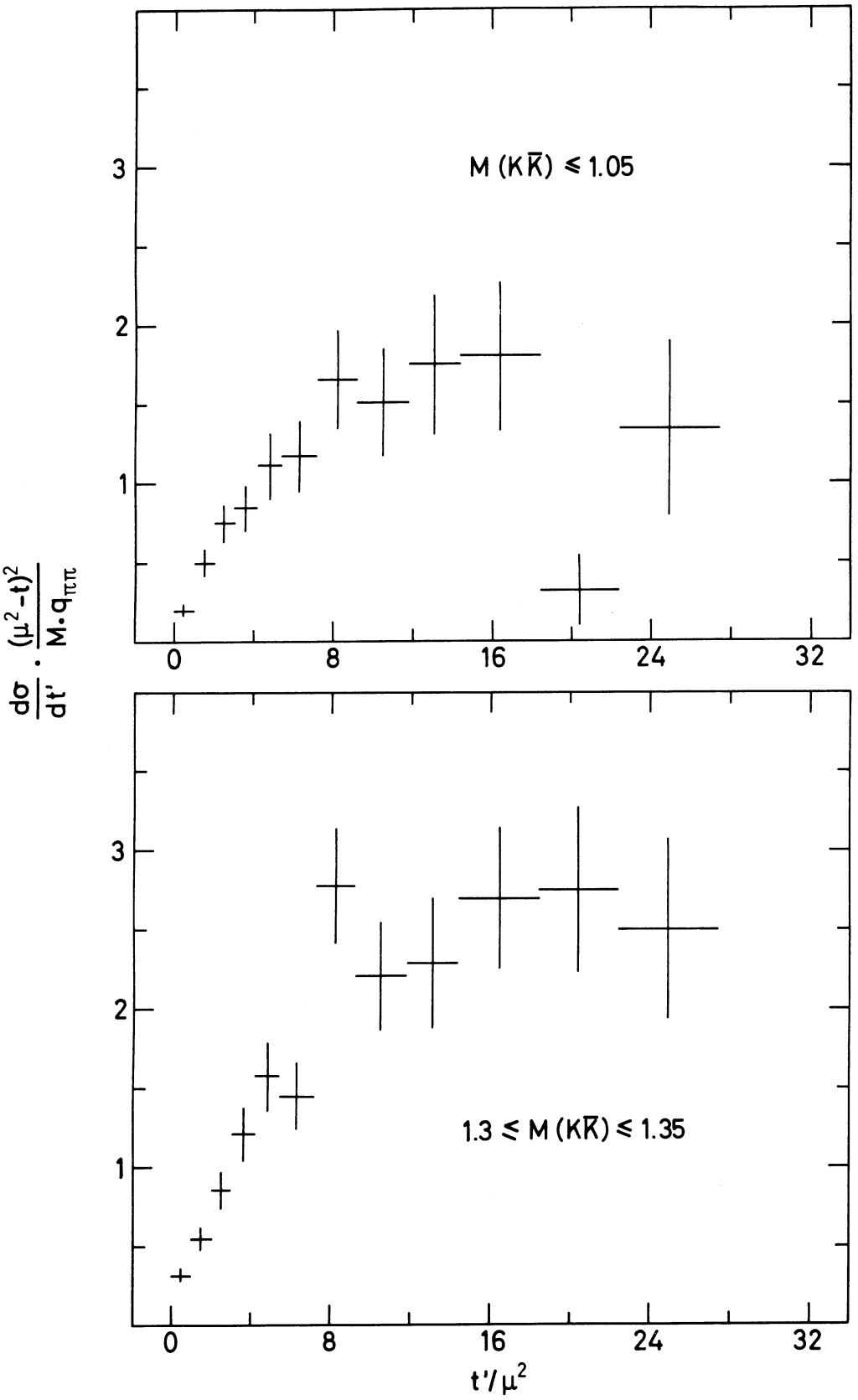
M (KK̄) ≤ 1.05
1.3 ≤ M (KK̄) ≤ 1.35
$\frac{d\sigma}{dt'} \cdot \frac{(\mu^2-t)^2}{M \cdot q_{\pi\pi}}$
t'/μ^2
0
8
16
24
32
1
2
3

Fig. 8

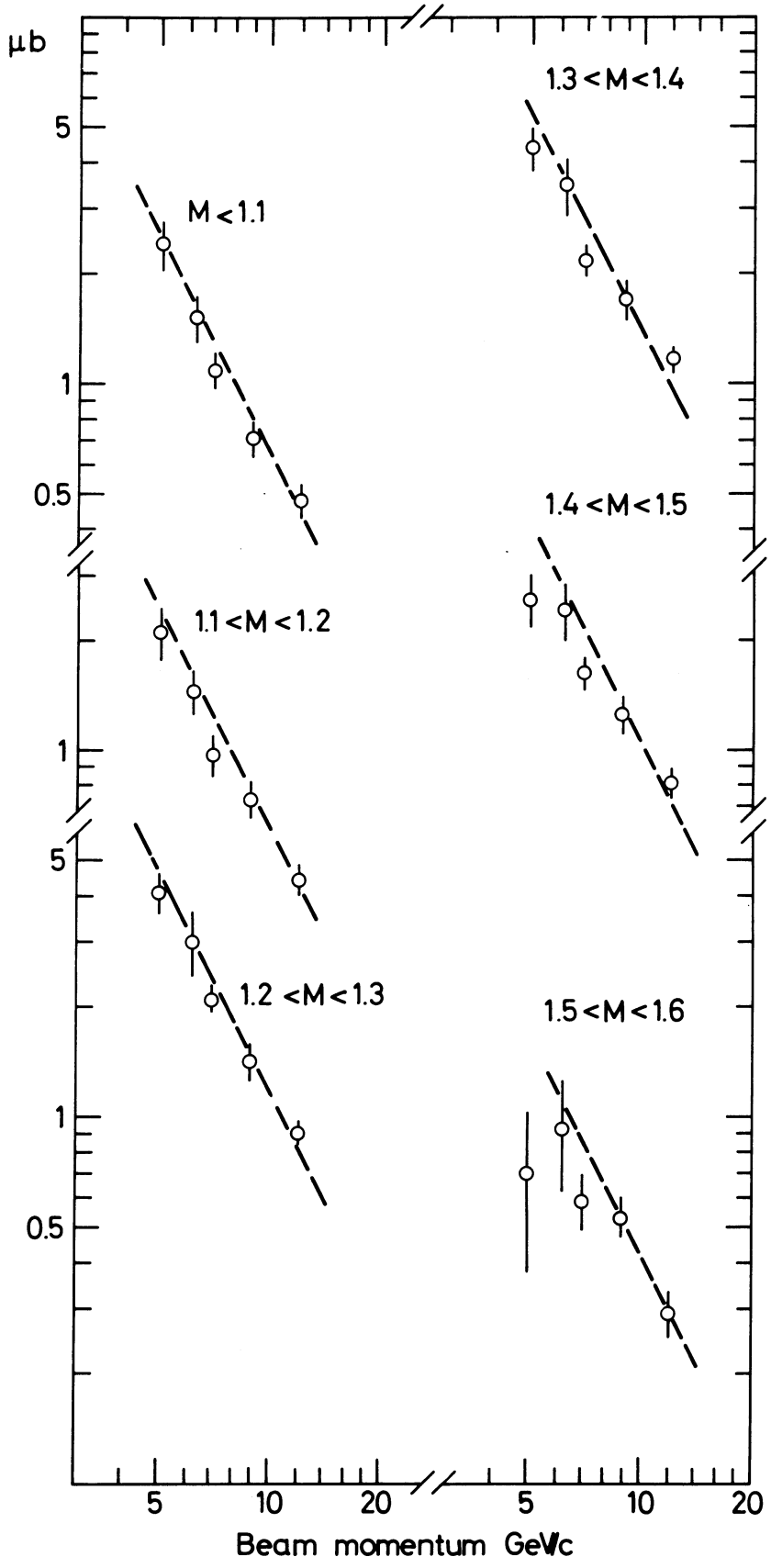
μb
5
1
0.5
M<1.1
1.1<M<1.2
1.2<M<1.3
1.3<M<1.4
1.4<M<1.5
1.5<M<1.6
5
10
20
Beam momentum GeV/c

Fig. 9

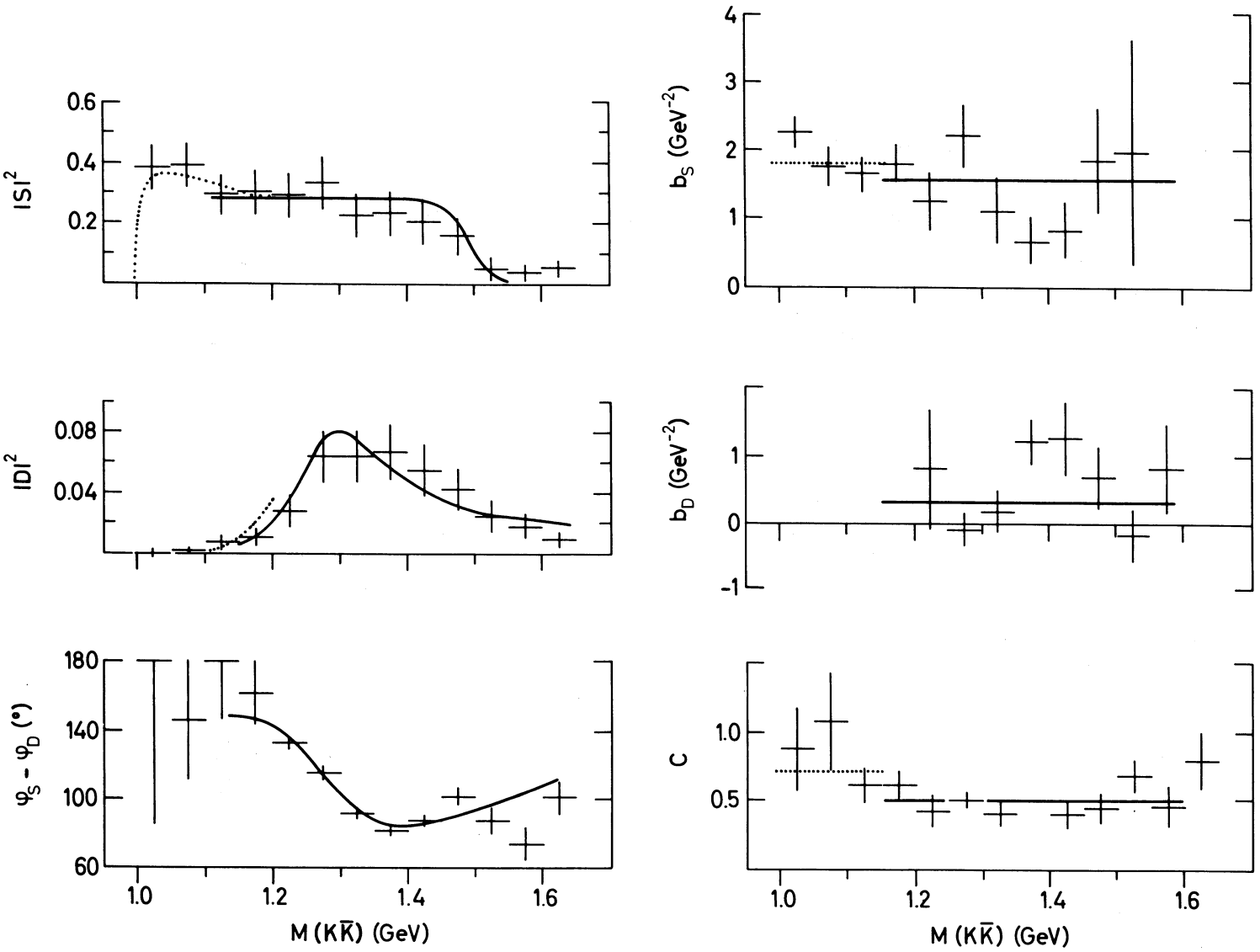

Fig. 10

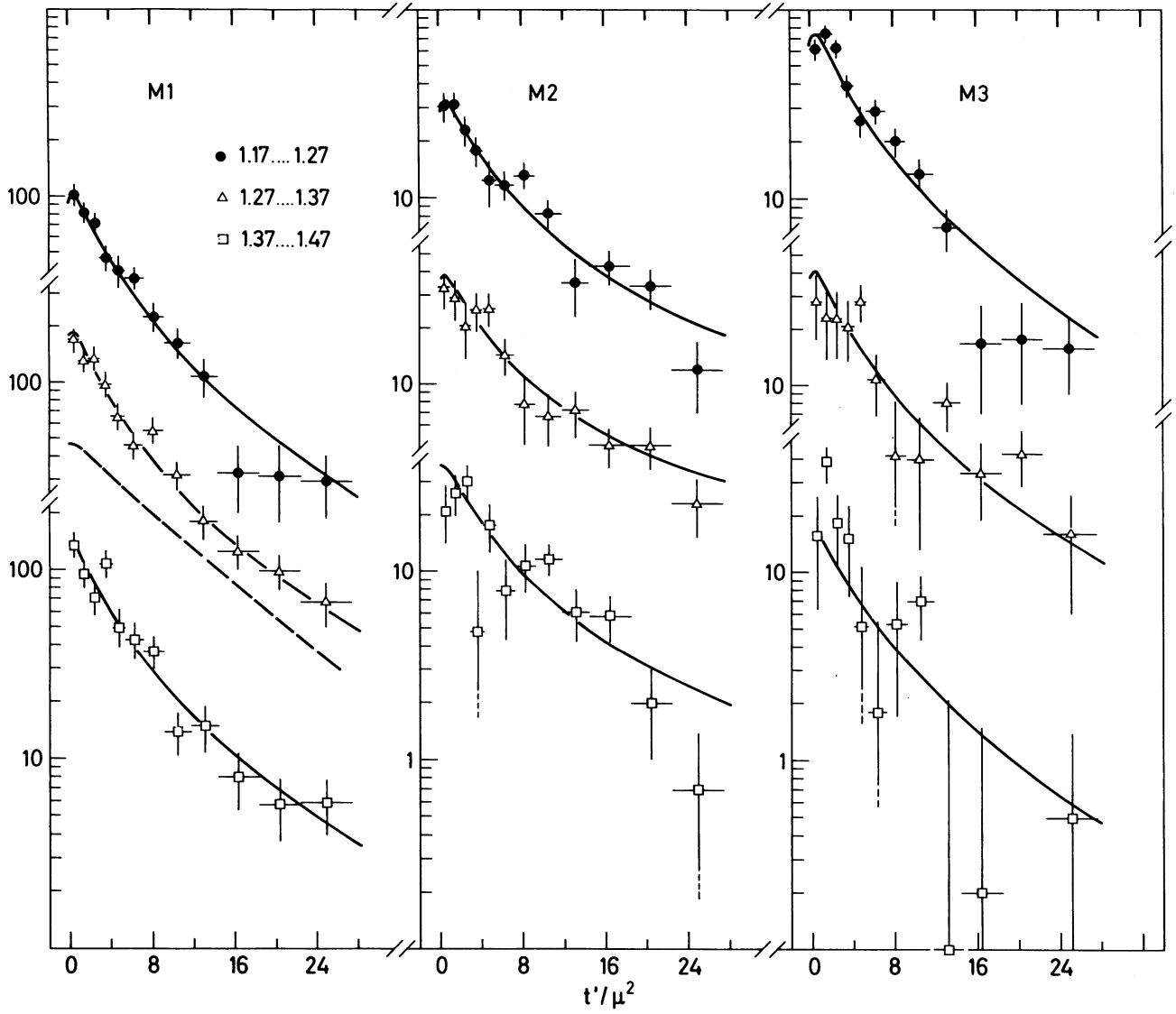

Fig. 11

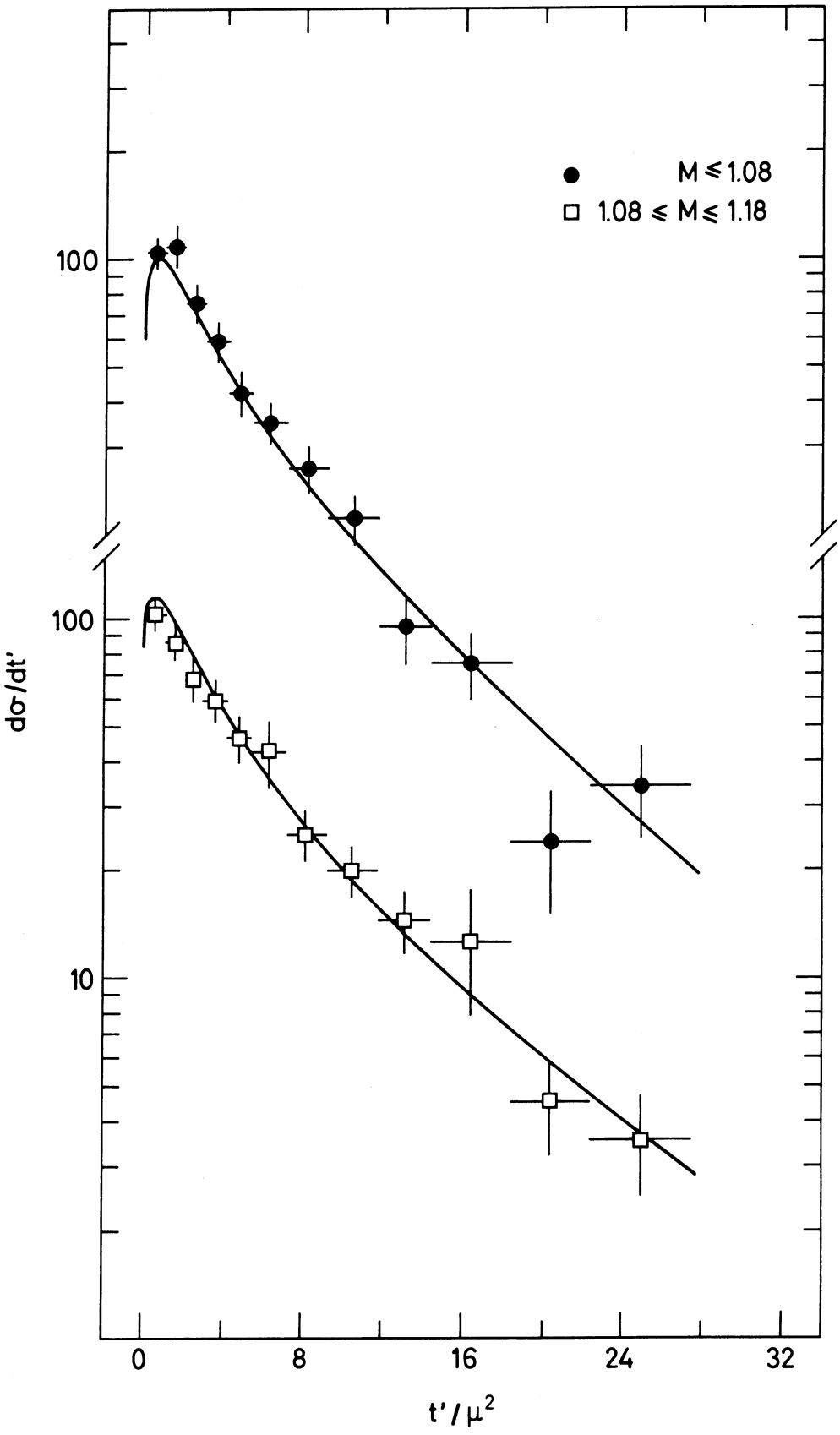

Fig. 12